A New Polarization-Based Vegetation Index to Improve the Accuracy of Vegetation Health Detection by Eliminating Specular Reflection of Vegetation

Siyuan Li, Jiannan Jiao, Jinbo Chen, and Chi Wang

***Abstract*— Monitoring the chlorophyll content changes in the plant via remote sensing is of great significance for understanding plant growth and monitoring vegetation pests and diseases, which is an important method to study the global climate change. However, the monitored information is often interfered by leaf specular reflection, resulting in reduced accuracy of chlorophyll content inversion. In this article, to eliminate the interference of specular reflection in vegetation remote sensing, a polarized multispectral imaging system (PMSIS) used in the different-light-level situation to observe vegetation was developed, and a new specular reflection removal vegetation index (NSRVI) was proposed to better detect the vegetation health condition under specular reflection interference. Based on previous studies, several vegetation indices (simple ratio (SR) index, normalized difference vegetation index (NDVI); modified simple ratio index (mSR), modified normalized difference vegetation index (mNDVI); polarization based simple ratio index (pSR), polarization based normalized difference vegetation index (pNDVI); and NSRVI) were established, and the impact of specular reflection on vegetation health detection was evaluated. Correlation analysis was done on relative chlorophyll content [soil and plant analyzer development (SPAD)], SR, NDVI, mSR, mNDVI, pSR, pNDVI, and NSRVI to understand their potential ability to eliminate specular interference. The results show that SR and NDVI have the highest sensitivity to specular reflection, and the other three methods can alleviate the adverse effects of specular reflection to varying degrees. It was observed that NSRVI was well-correlated with SPAD (coefficient of determination (R^2) = 0.899 and root-mean-square error (RMSE) = 6.16), highlighting the potential of NSRVI in eliminating specular reflection interference and identifying vegetation health condition. In summary, this method can effectively eliminate specular interference and improve the detection accuracy of vegetation health condition.**

***Index Terms*— Polarization, remote sensing, soil and plant analyzer development (SPAD), specular reflection, vegetation health monitoring, vegetation index.**

I. Introduction

THE physiological status of plants depends on their biochemical parameters, such as various pigments, nitrogen, and water [1], [2]. Therefore, the quantification of vegetation biochemical parameters can provide direct and effective information for the study of ecological processes, and remote sensing provides a good chance to monitor global ecological change [3], [4], [5]. As one of the main pigments of green plants, it is generally considered that the chlorophyll content is higher in healthy plants than that in unhealthy plants [6]. The level of chlorophyll in plant leaves can be used as an important indicator for the health condition of vegetation and its adaptation to surrounding environmental stress [7]. Therefore, monitoring chlorophyll content changes in the plant is of great significance for understanding plant growth and monitoring vegetation diseases and insect pests [8], [9], [10], [11], [12], [13].

The wet chemical method is adopted in the traditional measurement of chlorophyll content [14]. As a time-consuming and labor-intensive method, it has also drawbacks to destroy the plant and it is impossible to perform large-scale monitoring in real time [15]. Therefore, how to obtain plant physiological parameters in a timely, rapid, efficient, and reliable manner has become an important issue. With the development of multispectral and hyper-spectral remote sensing technology, it provides a fast, effective, and nondestructive data collection method and can quantitatively analyze the vegetation biochemical parameters based on the vegetation indices, especially plant chlorophyll content [16], [17], [18].

Using the red and near-infrared wavelengths of plants, many scholars have developed various vegetation indices to detect the growth and condition of vegetation [19]. Vegetation indices can be mainly classified into ratio form [simple ratio (SR)] [20], normalized form [normalized difference vegetation index (NDVI)] [21], and other forms of chlorophyll sensitivity indices [22], [23], [24], [25], [26], [27], [28], [29], [30], [31]. Lichtenthaler et al. [32] found that the reflectance around 550 and 700 nm is most sensitive to the chlorophyll content of plants, and they introduced two ratio vegetation indices, which can be used for accurate estimation of chlorophyll content. However, when the reflectivity of the red wavelength is very small, the ratio vegetation index will be very large. Therefore, Rouse et al. [21] proposed the normalized vegetation index NDVI for this phenomenon, which is widely used in vegetation remote sensing. Yagci et al. [33] used a vegetation condition index (VCI) derived from NDVI to verify the effects of corn and soybean rotation. Liu et al. [34] used three NDVI indicators to detect the growth status (greening and browning)

Manuscript received 2 May 2022; revised 25 August 2022; accepted 24 September 2022. Date of publication 3 October 2022; date of current version 27 October 2022. This work was supported in part by the National Natural Science Foundation of China under Grant 62175144 and in part by Shanghai Science and Technology Innovation Action Plan under Grant 20142200100. *(Corresponding authors: Jiannan Jiao; Chi Wang.)*

The authors are with the Department of Precision Mechanical Engineering, Shanghai University, Shanghai 200444, China (e-mail: lsyyj@shu.edu.cn; m160018@e.ntu.edu.sg; jbchen@shu.edu.cn; wangchi@shu.edu.cn).

Digital Object Identifier 10.1109/TGRS.2022.3211503

of alpine vegetation (2001–2015). In addition, there are some other forms of vegetation indices that can also be applied to estimate plant chlorophyll content well under different situations. For instance, Datt [35] developed a three-band differential ratio vegetation index $(R_{850}-R_{710})/(R_{850}-R_{680})$, and it is believed that the index can help eliminate the effect of leaf surface scattering and thus have a higher sensitivity to chlorophyll content.

The main advantage of the above vegetation indices is their sensitivity to changes in the chlorophyll content. However, these vegetation indices may be affected by the specular reflection of leaf, affecting the inversion accuracy of chlorophyll content based on them. In remote sensing methods, reflectivity data often play an essential role and the reflection information of leaves includes two components [36]: one is the single scattering (i.e., specular reflection) that occurs on the leaf surface, and the other is multiple scattering (i.e., diffuse reflection) that passes through the interior of leaves [37], [38]. The specular reflection does not enter the interior of leaves and is related to cytochrome, cell wall, or water, so it has nothing to do with the biochemical characteristics of leaves [39]; hence, the specular reflection is considered to be a factor that reduces the estimation accuracy of leaf biochemical parameters.

To overcome the drawbacks of the specular reflection, Sims and Gamon [40] subtracted the leaves reflectance value at $R_{445\ \mathrm{nm}}$ from the original reflectance and developed improved SR [modified simple ratio index (mSR)] and ND (mND) indices, achieving better accuracy in chlorophyll estimation. Féret et al. [41] performed poor simulations of eucalyptus leaf reflectance with the PROSPECT-D model and recommended that specular reflection be specifically considered in future studies. Barry and Newnham [42] noticed interference caused by specular reflection of leaves when using PROSPECT-5 to extract carotenoid content from eucalyptus leaves. Xie et al. [43] measured the scattering distribution of maize leaves and found that the surface reflection of leaves was non-Lambertian, and the specular reflection of maize leaves could reach 50% in the visible light band. Some scholars proposed that the waxy layer on leaves would affect the simulation accuracy of the PROSECT 5 model and believed that the presence of the waxy layer was the main source of error in the estimation of pigment content in eucalyptus leaves [44]. Li et al. [45] carried out experiments on mucuna, paper mulberry, and ginkgo, proving that leaves with a different surface roughness has a certain degree of specular reflection. And they believe that the existence of specular reflection will affect the chlorophyll inversion accuracy. When the specular reflection is eliminated, the chlorophyll inversion accuracy is improved. Wang et al. [46] removed the specular reflection by identifying the highlight area, removing the highlight area and complementing it with surrounding information. Some scholars proposed to use wavelet transform to remove specular reflection components in remote sensing images, and it has been proven that wavelet transform is indeed effective for removing specular reflection [47], [48]. Although many of the above studies have attempted to directly remove or mitigate the specular interference of leaves, none of them explicitly evaluate the specular interference of leaves and introduce a vegetation index that removes the specular interference of leaves.

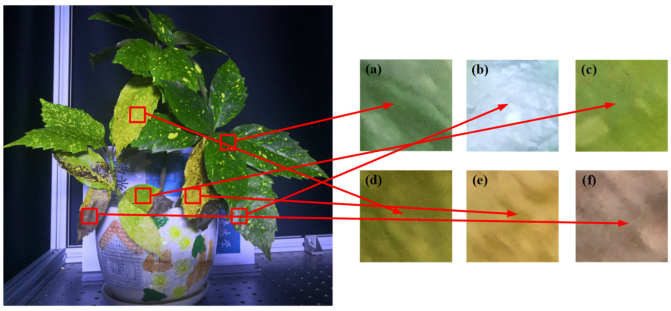

Fig. 1. Plant materials. A spotted laurel: (a)–(f) are the healthy leaf area, specular reflection leaf area, stressed grade-1 leaf area, stressed grade-2 leaf area, stressed grade-3 leaf area, and the withered leaf area, respectively.

TABLE I
STRESS GRADE CLASSIFICATION OF SPOTTED LAUREL

Stress grade	Symptoms
Healthy leaf	Green leaf
Specular reflection of leaf	Specular reflection (healthy leaf)
Stressed grade-1 leaf	Slight yellowing
Stressed grade-2 leaf	Moderate yellowing
Stressed grade-3 leaf	Severe yellowing
Withered leaf	Completely withered

This study mainly aims to eliminate specular reflection interference and adopt remote sensing to detect the vegetation condition based on previous studies. Therefore, to get images of plants at $R_{445\ \mathrm{nm}}$, $R_{680\ \mathrm{nm}}$, and $R_{760\ \mathrm{nm}}$, we developed a polarized multispectral imaging system (PMSIS), polarized images at angles of 0, 60, 120, and introduced new specular reflection removal vegetation index (NSRVI) to eliminate the specular reflection interference of plants and improve the detection accuracy of vegetation health condition. Correlation analysis was performed between SR, NDVI, mSR, modified normalized difference vegetation index (mNDVI), polarization based simple ratio index (pSR), polarization based normalized difference vegetation index (pNDVI), and NSRVI with plant chlorophyll content [soil and plant analyzer development (SPAD)] to ascertain their potential to eliminate specular reflection interference, and the corresponding test results were given. Furthermore, with our innovative research in ground-based remote sensing, it is expected that the platform will be transformed into an air- and space-based one in the future for large-scale applications.

II. PLANT MATERIALS AND METHODS

A. Plant Materials

In this study, the polarization and spectral image for analysis came from a plant at Shanghai University, Shanghai, China—spotted laurel (Aucuba japonica). As shown in Fig. 1, the spotted laurel had different healthy situations. Fig. 1(a)–(f) are defined as healthy leaf area, leaf specular reflection area (healthy leaf), stressed grade-1 leaf area, stressed grade-2 leaf area, stressed grade-3 leaf area, and withered leaf area. The classification of stress grades is shown in Table I.

In this study, we developed a PMSIS, collecting polarization and spectral image data of spotted laurel. In order to verify

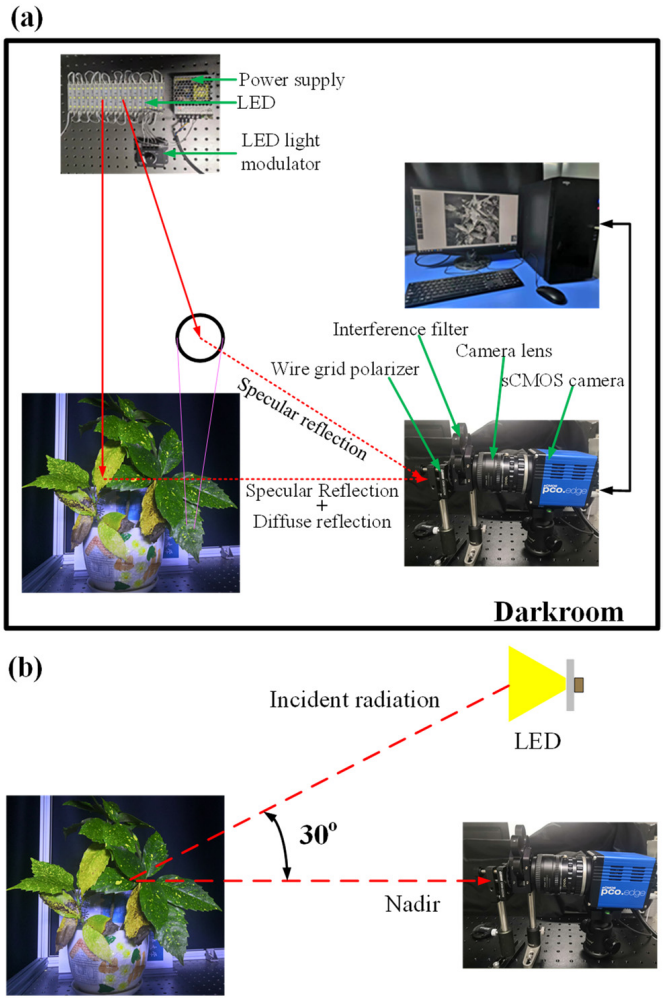

Fig. 2. (a) Polarized multispectral low-light-level imaging system. (b) Measurement direction.

the ability to specular reflection, SPAD values of leaves under different health conditions were measured and fit with vegetation index. Finally, experiments were carried out on a pot of spotted laurel under different illuminations, namely, 0.27, 1.19, 5.13, 10.29, and 102.1 lx in the dark room of the laboratory to verify the stability of the system.

B. Design of Imaging System

Our previous work studied the application of detecting the vegetation condition through remote sensing during the nighttime outdoors [49]. Based on PMSIS, a new method of night plant status detection was proposed to detect vegetation to better monitoring of plant health in the nighttime environment. In this article, the PMSIS was developed based on the hardware of previous studies, including a scientific sCMOS camera (PCO. Edge 4.2) with 2048 pixels ×2048 pixels, filters installed on a rotary filter mount, and a linear polarizer installed on a rotary polarizer mount. To be specific, we use blue light band filters from Semrock (FF01-445/20-25) and band filters from Thorlabs [(FB680-10, red) and (FB760-10, near-infrared)].

The PMSIS is shown in Fig. 2(a). In order to simulate different illumination environments, the system is placed in a dark room made of optical shading materials, with a shading rate greater than 99%. During the experiment, the illuminance of the darkroom was controlled to be 0.27, 1.19, 5.13, 10.29, and 102.1 lx, respectively. We carried out the experiment at Shanghai University in winter (longitude, latitude: 121°24′ 1.95″, 31°19′ 10.57″). As shown in Fig. 2(b), to verify the feasibility of the new method, a randomly selected incident zenith angle (30°) was applied. The measurement is carried out in the direction of the nadir because the direction of the nadir is the conventional observation direction in remote sensing.

C. Measurement of SPAD Content

A hand-held chlorophyll meter (Medium Kelvin, TYS-4N) was used to measure SPAD of different health conditions. Fifty readings were recorded on leaves of each stress grade, and the average value was taken as the reference value for SPAD. During the test, light was emitted in two bands from two LED light sources: one is red (center wavelength: 650 nm), and the other is infrared (center wavelength: 940 nm). The two bands of light got through the leaves and were received and calculated.

D. Data Acquisition and Analysis

The sCMOS camera and filters with bands of $R_{445\ \mathrm{nm}}$, $R_{680\ \mathrm{nm}}$, and $R_{760\ \mathrm{nm}}$ were used to collect the spectral image of plants, and a polarizer was used to collect the polarization image of plants at 0°, 60°, and 120°, with the linear polarization of vegetation being calculated. In this study, the spectral analysis focused on chlorophyll absorption characteristics near 680 nm and chlorophyll reflection characteristics near 760 nm in the central band, and seven vegetation indices, including SR, NDVI, mSR, mNDVI, pSR, pNDVI, and NSRVI, were developed to invert vegetation health condition.

1) Measurement of DoLP of Vegetation: Light scattered by surfaces of the vegetation is partly polarized [50], [51], [52], which is a combination of randomly polarized radiation and polarized radiation. To check the polarization information, the Stokes vector-based method can be realized via a simple set of measurements of the irradiance transmitted through a conceptual set of polarized filters [53], [54], and the Stokes parameters are defined as

$$F = \begin{bmatrix} I \\ Q \\ U \\ V \end{bmatrix} = \begin{bmatrix} \langle A_x^2 + A_y^2 \rangle \\ \langle A_x^2 - A_y^2 \rangle \\ \langle 2A_x A_y \cos\gamma \rangle \\ \langle 2A_x A_y \sin\gamma \rangle \end{bmatrix} = \begin{bmatrix} S_0 \\ S_1 \\ S_2 \\ S_3 \end{bmatrix}. \quad (1)$$

The parameters (commonly denoted by I, Q, U, V) can be fully describe the polarization information related with a beam. For a beam, the S_0 term describes the total energy, the S_1 term describes the linear horizontal or vertical polarization information, the S_2 term describes linear ±45° polarization information, and the S_3 term describes right- or left-handed circular polarization information.

For the passive remote sensing in nature, the circularly polarized information is usually so small that polarization

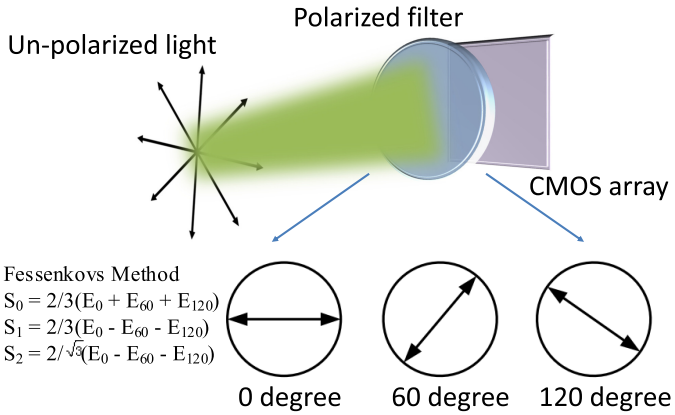

Fig. 3. Characterization of Stokes vectors based on the Fessenkovs method. E stands for the detected energy through polarizers of a certain angle.

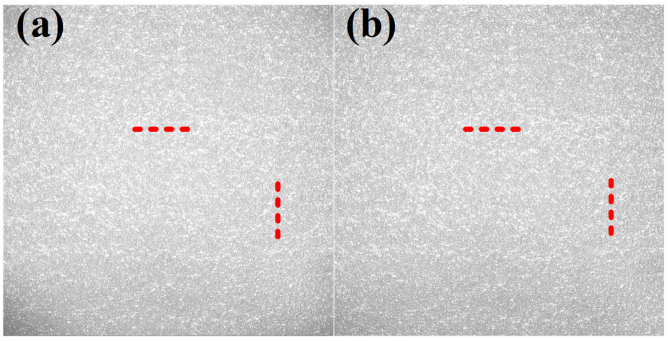

Fig. 4. (a) Image of I component of stokes. (b) General intensity.

state of a beam can be characterized by linear degree of polarization (DoLP), which has a relationship with polarized reflectance (R_p) and bidirectional reflectance factor (BRF), expressed as [55]

$$\text{DoLP} = \frac{R_P}{\text{BRF}}. \tag{2}$$

The DoLP can be calculated based on the Stokes parameters

$$\text{DoLP} = \frac{\sqrt{S_1^2 + S_2^2}}{S_0}. \tag{3}$$

As shown in Fig. 3, the Fessenkovs method was used to filter the incident radiation to measure the linear Stokes parameters and obtain DoLP.

The relative accuracy of PMSIS was checked based on the first parameter S_0 (denoted by I) of Stokes, which should be the general detected energy without the polarization filter and obtained by

$$S_0 = \frac{2}{3}(E_0 + E_{60} + E_{120}). \tag{4}$$

Fig. 4 shows the comparison between the direct measurement without a polarization filter and the I component measurement: Fig. 4(a) is the image of I component of stokes and Fig. 4(b) is the general intensity. The dashed lines are the randomly selected interest regions for comparison, as shown in Fig. 5. It shows that the I component is linear to the general intensity of direct measurement and the relative accuracy of

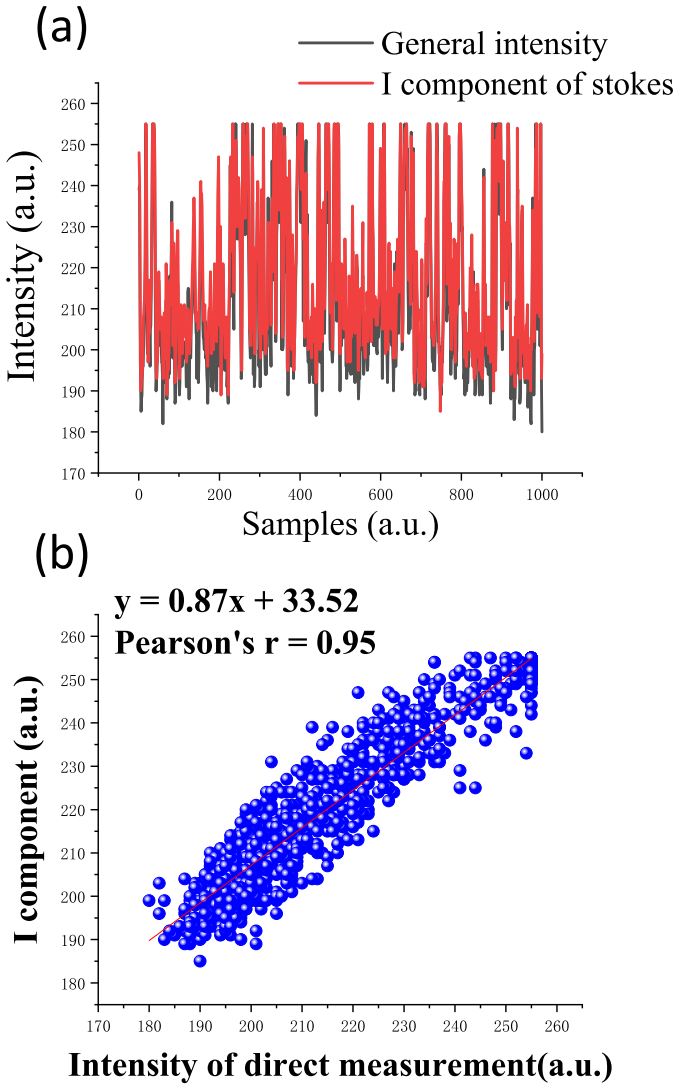

Fig. 5. Comparison between general intensity of direct measurement and I component: (a) Intensities of interest regions and (b) comparison of intensities from direct measurement and I component.

the polarization measurement is reliable. Pearson's r was calculated to check the correlation between direct measured intensity and I component of stokes, with a value of 0.95.

2) Selection and Construction of Vegetation Index: Of the vegetation indices for estimating chlorophyll content that have been used in the literature, many are variations of SR or normalized difference (NDVI) indices. We screened and classified the vegetation indices appropriately, focusing on their potential to be insensitive to leaf specular reflectance. SR and NDVI indicators are widely used as they are simple to calculate and involve not many bands. The calculation formula is as follows. The wavelengths of λ_1 and λ_2 in this article are $R_{760\ \text{nm}}$ and $R_{680\ \text{nm}}$, respectively,

$$\text{SR} = \frac{R_{\lambda 1}}{R_{\lambda 2}} \tag{5}$$

$$\text{NDVI} = \frac{(R_{\lambda 1} - R_{\lambda 2})}{(R_{\lambda 1} + R_{\lambda 2})} \tag{6}$$

where $R_{\lambda 1}$ and $R_{\lambda 2}$, respectively, represent the reflectance values at the wavelengths of λ_1 and λ_2. In (5), a constant b is added to $R_{\lambda 1}$ and $R_{\lambda 2}$. When $R_{\lambda 1} \neq R_{\lambda 2}$, then $R_{\lambda 1}/R_{\lambda 2}$ is not

equal to $(R_{\lambda 1}+b)/(R_{\lambda 2}+b)$. This shows that the SR index is more sensitive to the specular reflectance. Similarly, the NDVI index is also sensitive to specular reflection reflectance. The correction strategy proposed by Sims and Gamon [40] can be applied to reduce the sensitivity to specular reflectivity of the SR and NDVI indices, and the formulas are as follows:

$$\mathrm{mSR} = \frac{(R_{\lambda 1} - R_{445\ \mathrm{nm}})}{(R_{\lambda 2} - R_{445\ \mathrm{nm}})} \tag{7}$$

$$\mathrm{mNDVI} = \frac{(R_{\lambda 1} - R_{\lambda 2})}{(R_{\lambda 1} + R_{\lambda 2} - 2R_{445\ \mathrm{nm}})}. \tag{8}$$

As assumed by Sims and Gamon [40], $R_{445\ \mathrm{nm}}$ is the specular reflectance. Specular reflectance ($R_{445\ \mathrm{nm}}$) is removed from $R_{\lambda 1}$ and $R_{\lambda 2}$, so mSR and mNDVI are not sensitive to specular reflectance.

In addition, the inversion accuracy of leaf chlorophyll can be improved with the polarization measurement method proposed by Li et al. [45] to remove specular reflection on the leaf surface, described as follows.

First, the total reflectance (R) of a blade is the sum of the specular (R_{s}) and diffuse reflectance (R_{diff}) components

$$R = R_{\mathrm{s}} + R_{\mathrm{diff}}. \tag{9}$$

According to the Fresnel equation, when the angle of incidence is not 0° or 90°

$$R_{\mathrm{s}} = R_p \times c \tag{10}$$

where R_p is the leaf polarized reflectance. Equation (10) is established on the premise that specular reflection is the main source of polarized reflection, where c is the constant, and R_{s} can be regarded as the amplification of R_p in quantity. To get R_p, DoLP needs to be calculated first, and it is calculated by (3)

$$R_p = R \times \mathrm{DoLP}. \tag{11}$$

Since the infrared band is not sensitive to specular reflection, polarization removal is performed only on $R_{\lambda 2}$, where C is 1.2. The equation is as follows:

$$\mathrm{pSR} = \frac{R_{\lambda 1}}{(R_{\lambda 2} - 1.2R_{\lambda 2} \times \mathrm{DoLP})} \tag{12}$$

$$\mathrm{pNDVI} = \frac{[R_{\lambda 1} - (R_{\lambda 2} - 1.2R_{\lambda 2} \times \mathrm{DoLP})]}{[R_{\lambda 1} + (R_{\lambda 2} - 1.2R_{\lambda 2} \times \mathrm{DoLP})]}. \tag{13}$$

3) New Specular Reflection Removal Vegetation Index: For the spectral data, since the infrared band is not sensitive to specular reflection, we found that the spectral image of $R_{760\ \mathrm{nm}}$ is insensitive to specular reflection, while those of $R_{680\ \mathrm{nm}}$ and $R_{445\ \mathrm{nm}}$ are more sensitive to specular reflection in the experiment. Therefore, according to the correction strategy put forward by Sims and Gamon [40], we only need $R_{680\ \mathrm{nm}}$ minus $R_{445\ \mathrm{nm}}$. In addition, the polarization measurement method proposed by Li et al. [45] to remove the specular reflection on the leaf surface indicates that the specular reflection of leaf can be calculated from the polarized reflectance, which is calculated by DoLP. Therefore, this article combines the advantages of both and proposes the NSRVI. The equation is as follows:

$$\mathrm{NSRVI} = \frac{R_{760\ \mathrm{nm}} - (N \times R_{680\ \mathrm{nm}} - a \times R_{445\ \mathrm{nm}} - b \times \mathrm{DoLP})}{R_{760\ \mathrm{nm}} + (N \times R_{680\ \mathrm{nm}} - a \times R_{445\ \mathrm{nm}} - b \times \mathrm{DoLP})}. \tag{14}$$

In NSRVI, it is considered that the specular reflection interference can be determined by $R_{445\ \mathrm{nm}}$ and DoLP. The reflection at $R_{445\ \mathrm{nm}}$ is mainly from specular reflection and can be used to remove the specular reflection effects. To further improve the accuracy, the DoLP is considered. As DoLP is a relative ratio (2), a constant b is used to modify DoLP to has the same unit as the reflectance (R), and b works as the reflectance multiplied by a coefficient (same as $a \times R_{445\ \mathrm{nm}}$). Subtracting $R_{445\ \mathrm{nm}}$ from $R_{680\ \mathrm{nm}}$ can remove part of the specular reflection, and DoLP can be applied to further remove the specular reflection.

Based on the equation, $R_{445\ \mathrm{nm}}$ is regarded as specular reflection, which is subtracted from the reflectance at $R_{680\ \mathrm{nm}}$ to remove the specular reflection for that band. Since the image intensities of $R_{680\ \mathrm{nm}}$ and $R_{445\ \mathrm{nm}}$ are different, the specular reflection can be well-eliminated when the reflectance intensities of $R_{680\ \mathrm{nm}}$ and $R_{445\ \mathrm{nm}}$ are equal. In the experiment, the intensity of the image for $R_{445\ \mathrm{nm}}$ is about 1.5 times that of the $R_{680\ \mathrm{nm}}$, so $N = 1.5$ and $a = -1$ are used. To further eliminate the specular reflection, DoLP is used and the constant coefficient of b is determined as -1. The N value (1.5) is determined by the experiment and should be modified when observation situations are different, which has a direct impact on the removal of specular reflection.

E. Accuracy Evaluation and Verification

In this article, the coefficient of determination (R^2), bias (Bias), and root-mean-square error (RMSE) are applied to check the correlation level between vegetation index and chlorophyll. Among them, R^2 represents the closeness of the correlation. When R^2 is closer to 1, it indicates that the reference value of the related equation is higher; on the contrary, when it is closer to 0, it indicates that the reference value is lower. Bias reflects the error between the output of the model on the sample and the real value. The smaller the value is, the higher the accuracy of the model is. RMSE can reflect the degree of dispersion of the dataset. The smaller the value is, the higher the accuracy of the model is

$$R^2 = 1 - \frac{\sum_i \left(y_i - y_i'\right)^2}{\sum_i \left(y_i - \bar{y}\right)^2} \tag{15}$$

$$\mathrm{RMSE} = \sqrt{\frac{\sum_i \left(y_i - y_i'\right)^2}{n}} \tag{16}$$

$$\mathrm{Bias} = \frac{\sum_i \left(y_i - y_i'\right)}{n}. \tag{17}$$

F. Organization of This Study

In order to verify the effect of each vegetation index on removing specular reflection and the stability of the system

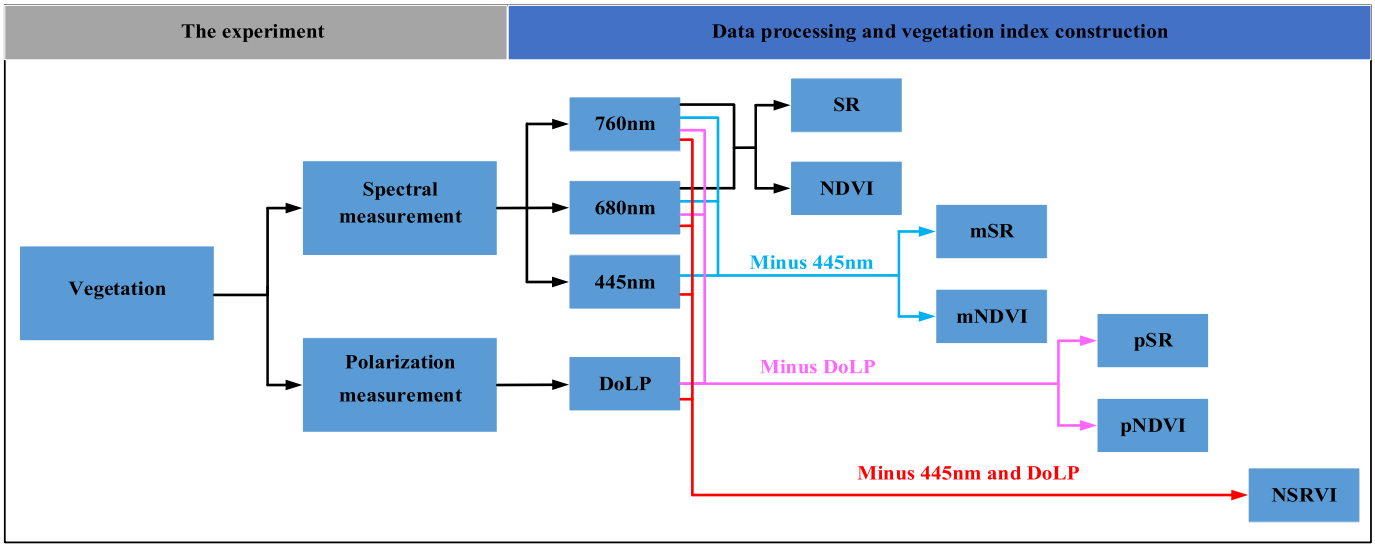

Fig. 6. Flowchart of this study.

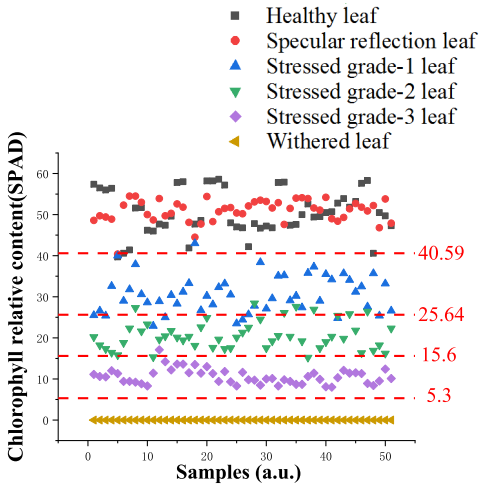

Fig. 7. Scatterplot of SPAD content.

under different illumination levels, in Section III-A, we measured the SPAD contents of spotted laurel of different health conditions. Section III-B introduces vegetation health detection of each vegetation indices and fitting with SPAD content. Section III-C presents the experimental results under different illumination to demonstrate the stability of the system. Section III-D introduces multiangle experimental check.

The flowchart of typical steps for predicting the SPAD content of spotted laurel in this study is shown in Fig. 6.

III. Results

A. Statistics of SPAD Content

The SPAD of spotted laurel in different health conditions was measured, and Fig. 7 shows a scatterplot of the average SPAD content of leaves in different health conditions of the plant. As the health of leaves declines, their pigments degrade gradually, and the value of chlorophyll reduces gradually. The SPAD content of healthy leaf and specular reflective leaf is above 40.59, the SPAD content of stressed grade-1 leaf is 25.64–40.59, the SPAD content of stressed grade-2 leaf is 15.5–25.22, the SPAD content of stressed grade-3 leaf is 5.3–15.5, and the SPAD content of withered leaf is below 5.3. The sensitivity (Se) and specificity (Sp) of different plant status and their respective positive predictive value (PPV) and negative predictive value (NPV) were calculated using the misclassification rate of the SPAD scatterplot, as shown in Table II.

B. Monitoring of Vegetation Health Condition

The experimental illuminance was measured as 102.1 lx with an illuminometer.

1) SR and NDVI Measurements: Fig. 8(a) shows the SR image calculated by (5), and Fig. 8(b) shows the pseudo-color image of Fig. 8(a). Fig. 8(c) shows the NDVI image calculated by (6), and Fig. 8(d) shows the pseudo-color image of Fig. 8(c). The black-box area in Fig. 8 is lower than the surrounding values due to specular reflection on the blade surface (see Section IV-A). The red-box area in Fig. 8 is withered leaf, and the values of withered leaf and stressed grade-3 leaf are not much different, so withered leaf and stressed grade-3 leaf are confused.

Scatterplots of discriminant functions were drawn for six health condition areas. Fig. 9(a) shows a 2-D scatter diagram of SR image, where x-axis represents the number of groups and y-axis represents the SR value. The classification lines are drawn at the mean of the health condition grades of plants. For example, classification lines drawn at 0.571, 0.199, 0.085, and 0.041 distinguish healthy leaf, stressed grade-1 leaf, stressed grade-2 leaf, stressed grade-3 leaf, and withered leaf, respectively. Fig. 9(b) shows a 2-D scatterplot of the NDVI image. The classification lines drawn at 0.818, 0.529, 0.287, and 0.193 distinguish healthy leaf, stressed grade-1 leaf, stressed grade-2 leaf, stressed grade-3 leaf, and withered leaf, respectively. It can be seen that the values of healthy leaf and stressed grade-1 leaf are quite different in the scatterplot, and

TABLE II
CLASSIFICATION ACCURACY OF PLANT HEALTH CONDITION OBTAINED BY SR, NDVI, MSR, MNDVI, PSR, PNDVI, NSRVI, AND SPAD HEALTH GRADE

	Health - Grade 1				specular - Grade 1			Grade 1 - Grade 2				Grade 2 - Grade 3				Grade 3 - Withered			
	Se	Sp	PPV	NPV	Se	Sp	PPV	NPV	Se	Sp	PPV	NPV	Se	Sp	PPV	NPV	Se	Sp	PPV	NPV
SR	1	1	1	1	0	0	0	0	1	1	1	1	1	0.98	0.98	1	0.65	0.66	0.67	0.65
NDVI	1	1	1	1	0	0	0	0	1	1	1	1	1	1	1	1	0.21	0.32	0.16	0.39
mSR	1	1	1	1	1	0.77	0.71	1	1	1	1	1	1	1	1	1	0	0	0	0
mNDVI	1	1	1	1	1	1	1	1	0.79	0.95	0.96	0.75	1	1	1	1	0.94	1	1	0.94
pSR	0.98	0.93	0.92	0.98	0.69	0.63	0.57	0.75	0.89	0.94	0.94	0.88	0.88	0.88	0.88	0.88	0.95	0.79	0.75	0.96
pNDVI	0.84	0.91	0.92	0.82	0.42	0.41	0.43	0.39	1	0.93	0.92	1	0.98	0.94	0.94	0.98	0.81	0.85	0.86	0.8
NSRVI	0.94	0.92	0.92	0.94	0.92	0.96	0.96	0.92	0.9	0.92	0.92	0.9	1	0.94	0.94	1	0.96	1	1	0.96
SPAD	0.98	0.98	0.98	0.98	0.98	0.98	0.98	0.98	0.86	0.85	0.84	0.86	0.98	0.96	0.96	0.98	1	1	1	1

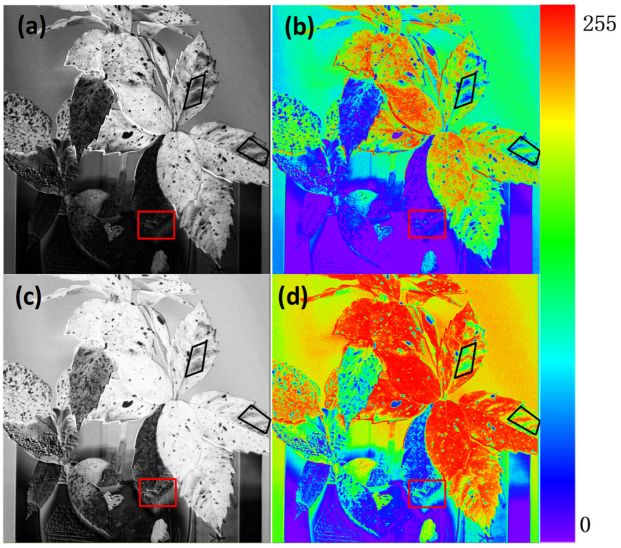

Fig. 8. Images recorded from spotted laurel: (a) SR image; (b) SR pseudo-color image; (c) NDVI image; and (d) NDVI pseudo-color image.

the specular reflected leaf is mistakenly regarded as stressed grade-2 leaf, while stressed grade-3 leaf and withered leaf are not clearly distinguished, which is the reason for the error of chlorophyll inversion using SR and NDVI. Based on the misclassification rate of the health condition of adjacent plants, we can determine the sensitivity and specificity of different vegetation condition and the PPV and NPV of the classification (Table II).

The linear correlation between SR and NDVI and SPAD was analyzed. As shown in Fig. 10(a) and (b), the correlation coefficient R^2 between SR and SPAD is 0.456, and that between NDVI and SPAD is 0.625. The correlation coefficient (R^2), RMSE, Bias, and P values are shown in Table III. All regression analyses were statistically significant ($p < 0.001$). The regression coefficients of all spectral features are rounded to three decimal places to avoid large rounding errors.

2) mSR and mNDVI Measurements: Fig. 11(a) shows the mSR image calculated by (7), and Fig. 11(b) shows the pseudo-color image of Fig. 11(a). Fig. 11(c) shows mNDVI image calculated by (8), and Fig. 11(d) shows a pseudo-color image of Fig. 11(c). The black-box area in Fig. 11 is higher than its surrounding values because the specular reflection of the blade is improved to high values with the correction strategy proposed by Sims and Gamon [40] (see Section IV-B). The specular reflection area is for the healthy leaf, so the accuracy of mSR and mNDVI for chlorophyll inversion is improved. In Fig. 11(a), the red-box area is withered leaf, and the value of the withered leaf is higher than that of the stressed grade-3 leaf, which is abnormal.

Fig. 12(a) shows a 2-D scatter diagram of mSR image, where x-axis represents the number of groups and y-axis represents the mSR value. The classification lines are drawn at the mean of the health condition grades of plants. For example, classification lines drawn at 0.656, 0.641, 0.464, and 0.253 distinguish healthy leaf, stressed grade-1 leaf,

TABLE III
CORRELATION COEFFICIENT (R^2), RMSE, BIAS, AND P VALUE

Type	Illuminance	R^2	RMSE	Bias	P
SR	102.1Lux	0.456	14.297	-0.0028	<0.001
NDVI	102.1Lux	0.625	11.862	-0.0005	<0.001
mSR	102.1Lux	0.726	10.143	0.0014	<0.001
mNDVI	102.1Lux	0.705	10.541	-0.0006	<0.001
pSR	102.1Lux	0.717	10.331	0.0094	<0.001
pNDVI	102.1Lux	0.751	9.682	-0.0015	<0.001
	102.1Lux	0.899	6.1603	0.0011	<0.001
	10.29Lux	0.855	7.3957	0.0008	<0.001
NSRVI	5.13 Lux	0.861	7.2493	-0.001	<0.001
	1.19 Lux	0.827	8.0782	0.002	<0.001
	0.27 Lux	0.8	8.6782	-0.0009	<0.001

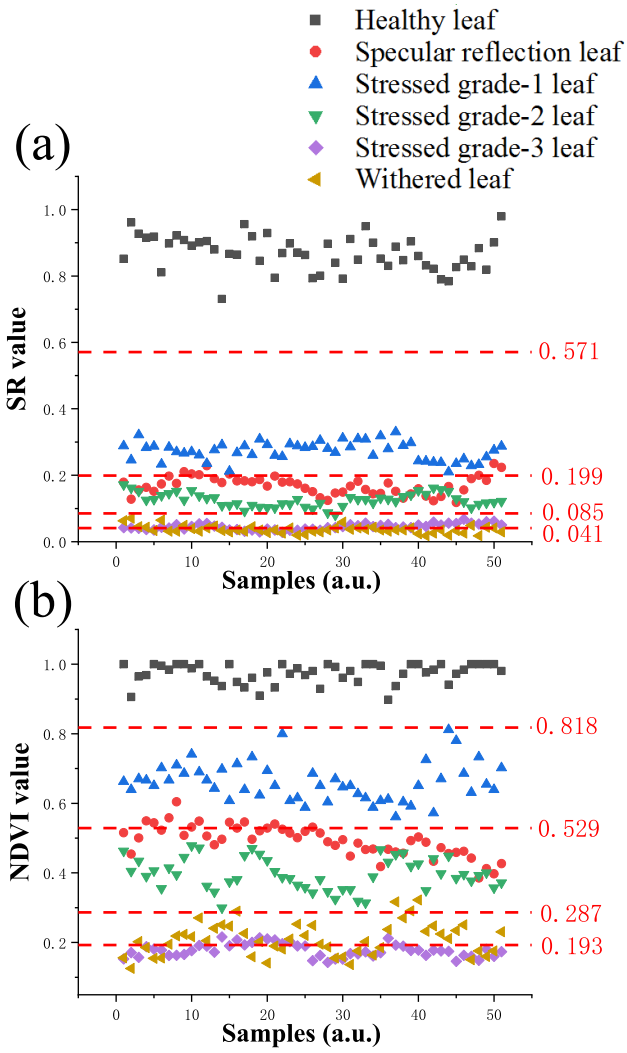

Fig. 9. Scatterplot: (a) SR scatterplot and (b) NDVI scatterplot. The classification lines are drawn at the mean of the health condition grades of plants of the adjoining groups.

stressed grade-2 leaf, stressed grade-3 leaf, and withered leaf, respectively. Fig. 12(b) shows a 2-D scatterplot of the mNDVI. The classification lines drawn at 0.464, 0.305, 0.223, and 0.114 distinguish healthy leaf, stressed grade-1 leaf, stressed grade-2 leaf, stressed grade-3 leaf, and withered leaf, respectively. It can be seen that the value of the specular reflection leaf is greater than that of the healthy leaf in the scatterplot (which should be equal in fact), while the value of the withered leaf is greater than that of stressed grade-3 leaf, which is a disadvantage of using mSR and mNDVI. Based on the misclassification rate of the health condition of adjacent plants, we can determine the sensitivity and specificity of different vegetation condition and the PPV and NPV of the classification (Table II).

The linear correlation between mSR and mNDVI and SPAD was analyzed. As shown in Fig. 13(a) and (b), the correlation coefficient R^2 between mSR and SPAD is 0.726, and that between mNDVI and SPAD is 0.705, with significantly improved accuracy. The correlation coefficient (R^2), RMSE, Bias, and P values are shown in Table III.

3) pSR and pNDVI Measurements: Fig. 14(a) shows the pSR image calculated by (12), and Fig. 14(b) shows the pseudo-color image of Fig. 14(a). Fig. 14(c) shows the pNDVI image calculated by (13), and Fig. 14(d) shows the pseudo-color image of Fig. 14(c). The pixel values of the black-box area in Fig. 14 and the surrounding area are of little difference because the specular reflection of the blade is improved to a higher value with the method proposed by Li et al. (2018). The specular reflection area is for the healthy leaf, so the chlorophyll inversion accuracy with improved mSR and mNDVI is improved. The withered leaf value in the red box is lower than the stressed grade-3 leaf, which is an improvement of this method.

Fig. 15(a) shows a 2-D scatter diagram of pSR image, where x-axis signifies the number of groups and y-axis signifies the pSR value. The classification lines are drawn at the mean of the health condition grades of plants. For example, the classification line drawn at 0.339 distinguishes healthy leaf from stressed grade-1 leaf, that drawn at 0.297 distinguishes specular reflection leaf from stressed grade-1 leaf, and those drawn at 0.226, 0.142, and 0.069 distinguish stressed grade-1 leaf, stressed grade-2 leaf, stressed grade-3 leaf, and withered leaf, respectively. Fig. 15(b) shows a 2-D scatterplot of the pNDVI image. The classification line drawn at 0.658 distinguishes

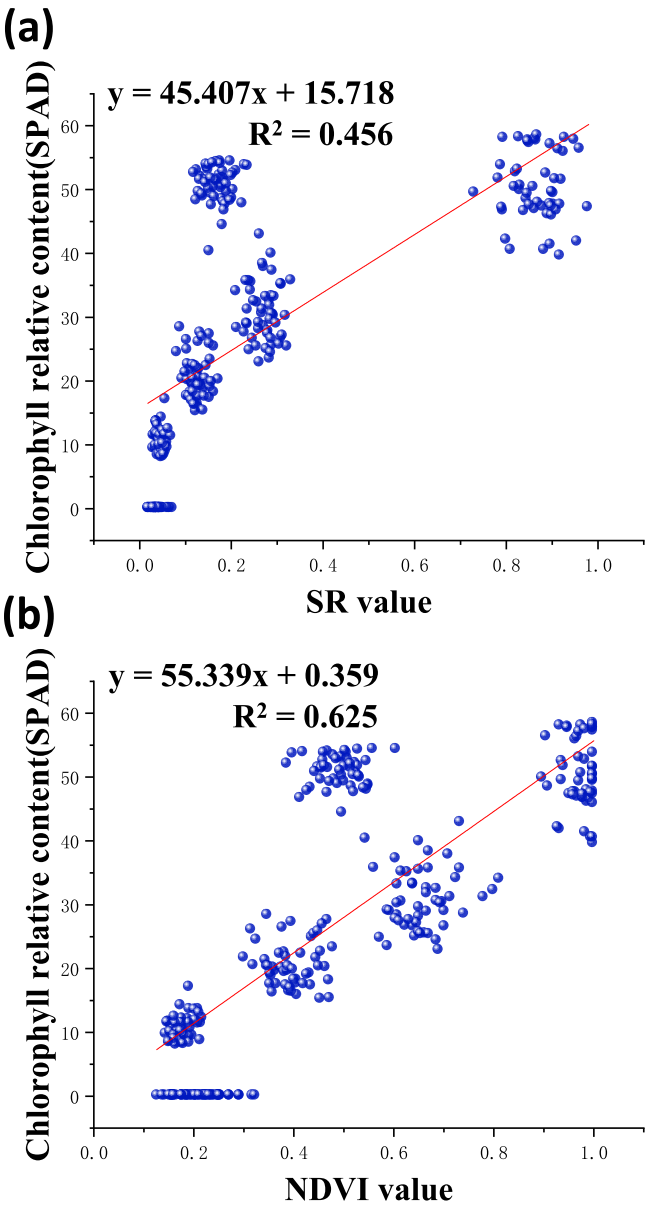

Fig. 10. (a) Correlation of SPAD with SR. (b) Correlation of SPAD with NDVI. Spotted laurel under varying degrees of health condition from healthy leaf and specular reflection leaf to grades 1–3 ($N = 51$).

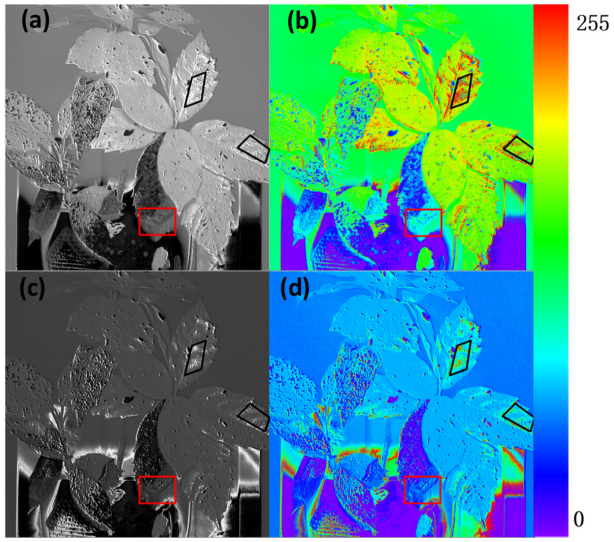

Fig. 11. Images recorded from spotted laurel: (a) mSR image; (b) mSR pseudo-color image; (c) mNDVI image; and (d) mNDVI pseudo-color image.

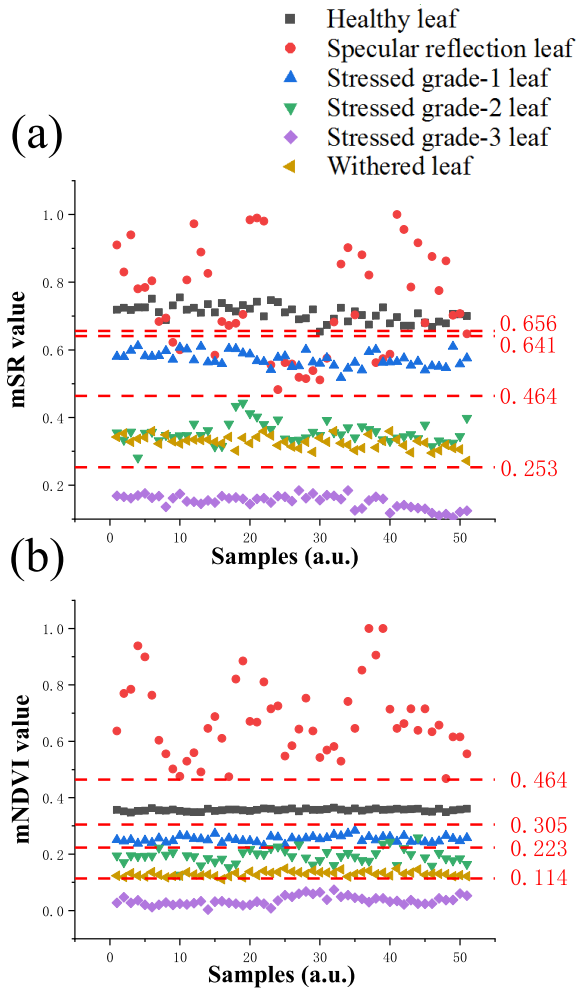

Fig. 12. (a) mSR scatterplot. (b) mNDVI scatterplot.

the healthy leaf and the stressed grade-1 leaf, that drawn at 0.565 distinguishes the specular reflection leaf and the stressed grade-1 leaf, and those drawn at 0.483, 0.298, and 0.155 distinguish stressed grade-1 leaf, stressed grade-2 leaf, stressed grade-3 leaf, and withered leaf, respectively. It can be seen that the values of specular reflection leaf in the scatterplot fluctuate greatly, but most of them are equal to the values of healthy leaf, which is an advantage of using pSR and pNDVI. Based on the misclassification rate of the health condition of adjacent plants, we can determine the sensitivity and specificity of different vegetation conditions and the PPV and NPV of the classification (Table II).

The linear correlation between pSR and pNDVI and SPAD was analyzed. As shown in Fig. 16(a) and (b), the correlation coefficient R^2 between pSR and SPAD is 0.717, and that between pNDVI and SPAD is 0.751. The inversion accuracy of pSR and pNDVI is significantly improved, and it is similar to that of mSR and mNDVI, which is also consistent with the results of previous studies [46]. The correlation coefficient (R^2), RMSE, Bias, and P values are shown in Table III.

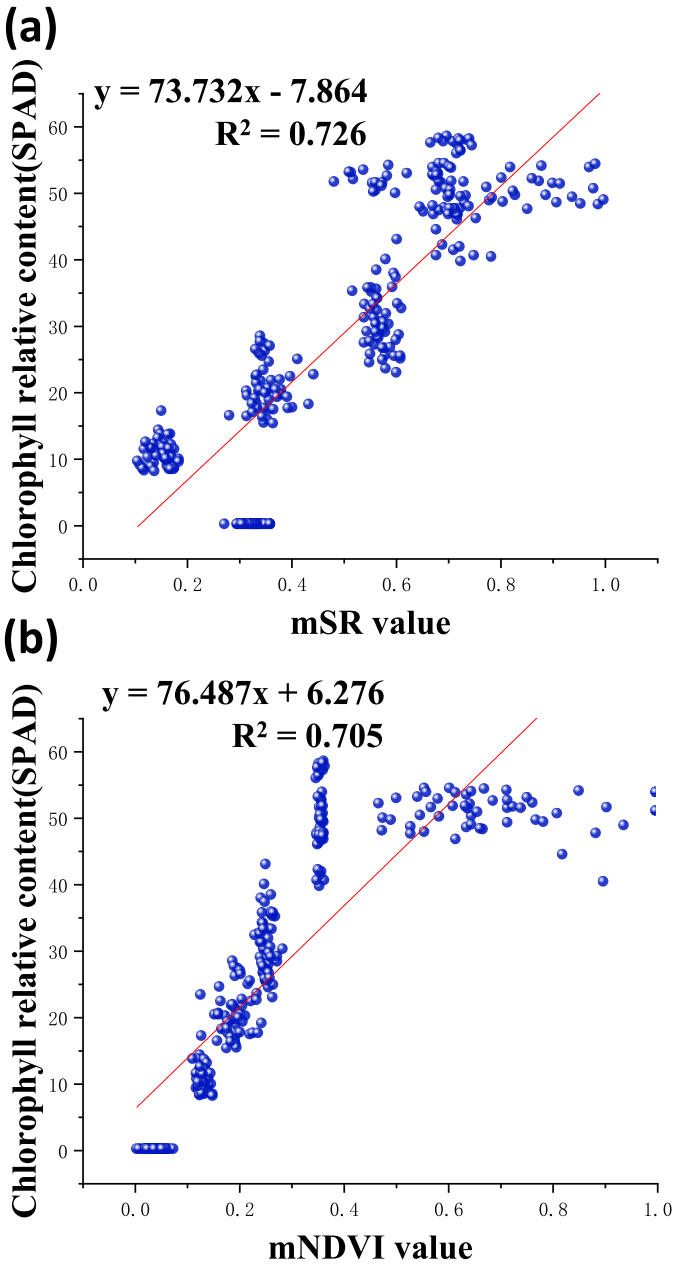

Fig. 13. (a) Correlation of SPAD with mSR. (b) Correlation of SPAD with mNDVI.

4) NSRVI Measurement: Fig. 17(a) shows the NSRVI image calculated by (14), and Fig. 17(b) shows the pseudo-color image of Fig. 17(a). In Fig. 17, the pixel values of the black-box area and the surrounding area are completely equal, and the value of the withered leaf in the red-box area is also lower than that of the stressed grade-3 area. Therefore, the accuracy of chlorophyll inversion by NSRVI has been improved significantly.

Fig. 18 shows a 2-D scatter diagram of NSRVI image, where x-axis signifies the number of groups, and y-axis signifies the NSRVI value. The classification lines are drawn at the mean of the health condition grades of plants. For example, the classification line drawn at 0.585 distinguishes healthy leaf from stressed grade-1 leaf, that drawn at 0.582 distinguishes specular reflection leaf from stressed grade-1 leaf, and those

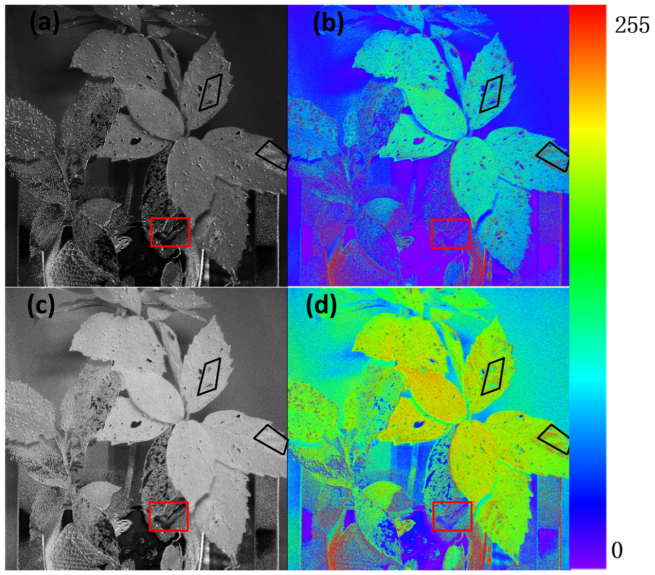

Fig. 14. Images recorded from spotted laurel: (a) pSR image; (b) pSR pseudo-color image; (c) pNDVI image; and (d) pNDVI pseudo-color image.

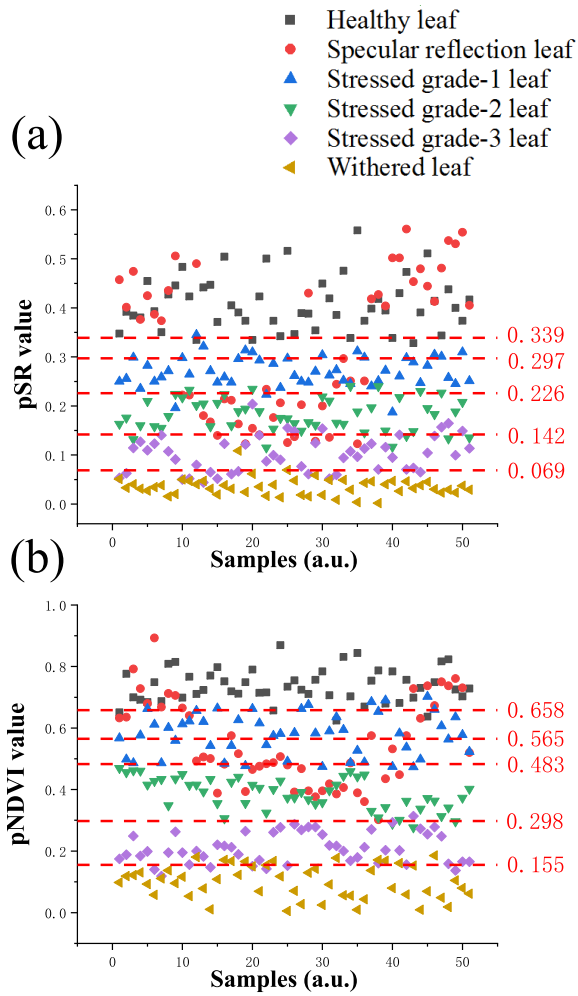

Fig. 15. (a) pSR scatterplot. (b) pNDVI scatterplot.

drawn at 0.401, 0.234, and 0.095 distinguish stressed grade-1 leaf, stressed grade-2 leaf, stressed grade-3 leaf, and withered leaf, respectively. In addition, the values of specular reflection

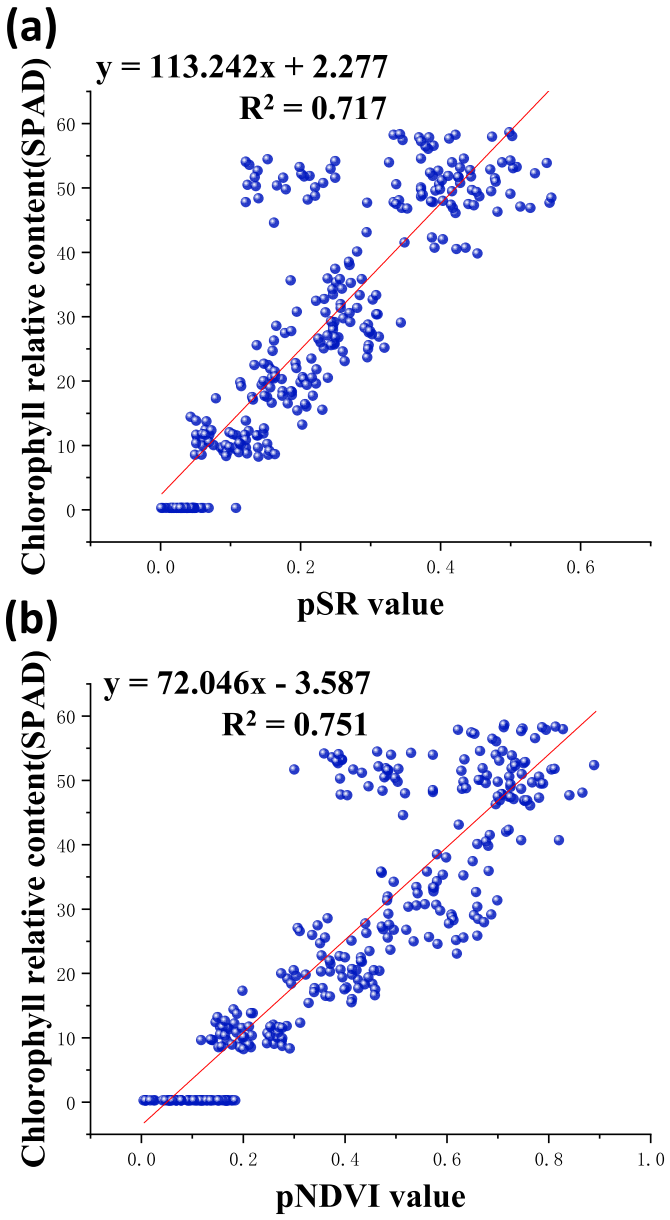

Fig. 16. (a) Correlation of SPAD with pSR. (b) Correlation of SPAD with pNDVI.

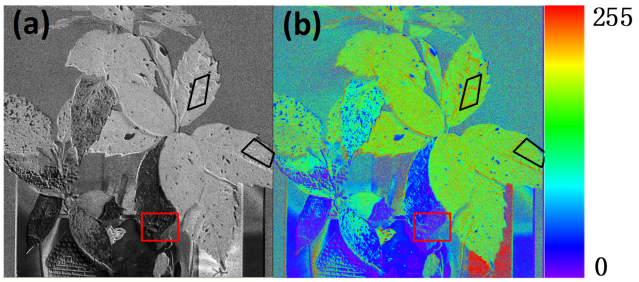

Fig. 17. Images recorded from spotted laurel: (a) NSRVI image and (b) NSRVI pseudo-color image.

leaf in the scatterplot are equal to those of healthy leaf, and the health condition grades of other plants are classified obviously. NSRVI greatly eliminates the interference caused by specular reflection and improves the accuracy of chlorophyll retrieval.

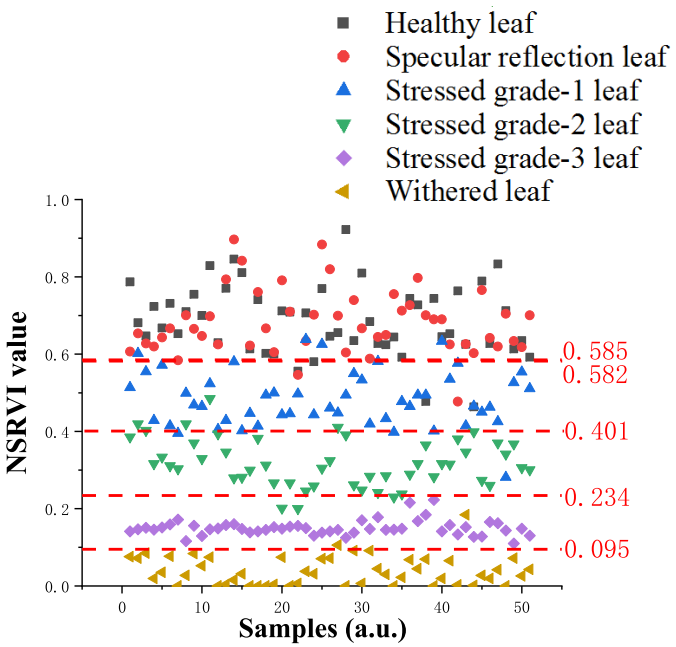

Fig. 18. NSRVI scatterplot.

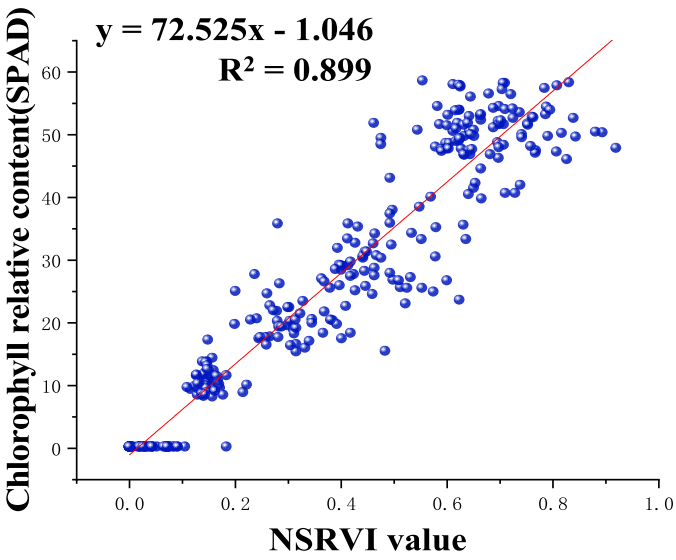

Fig. 19. Correlation of SPAD with NSRVI.

Based on the misclassification rate of the health condition of adjacent plants, we can determine the sensitivity and specificity of different vegetation conditions and the PPV and NPV of the classification (Table II).

The linear correlation between NSRVI and SPAD was analyzed. As shown in Fig. 19, the correlation coefficient R^2 between NSRVI and SPAD is 0.899. The chlorophyll inversion accuracy of NSRVI is greatly improved to a level better than those of mSR, mNDVI, pSR, and pNDVI. The correlation coefficient (R^2), RMSE, Bias, and P values are shown in Table III.

C. Experiments With Different Illuminance

A pot of spotted laurel was placed in the dark room, and the illuminance meter was used to measure the illuminance. In the experiment, there are five groups of illumination: 0.27, 1.19,

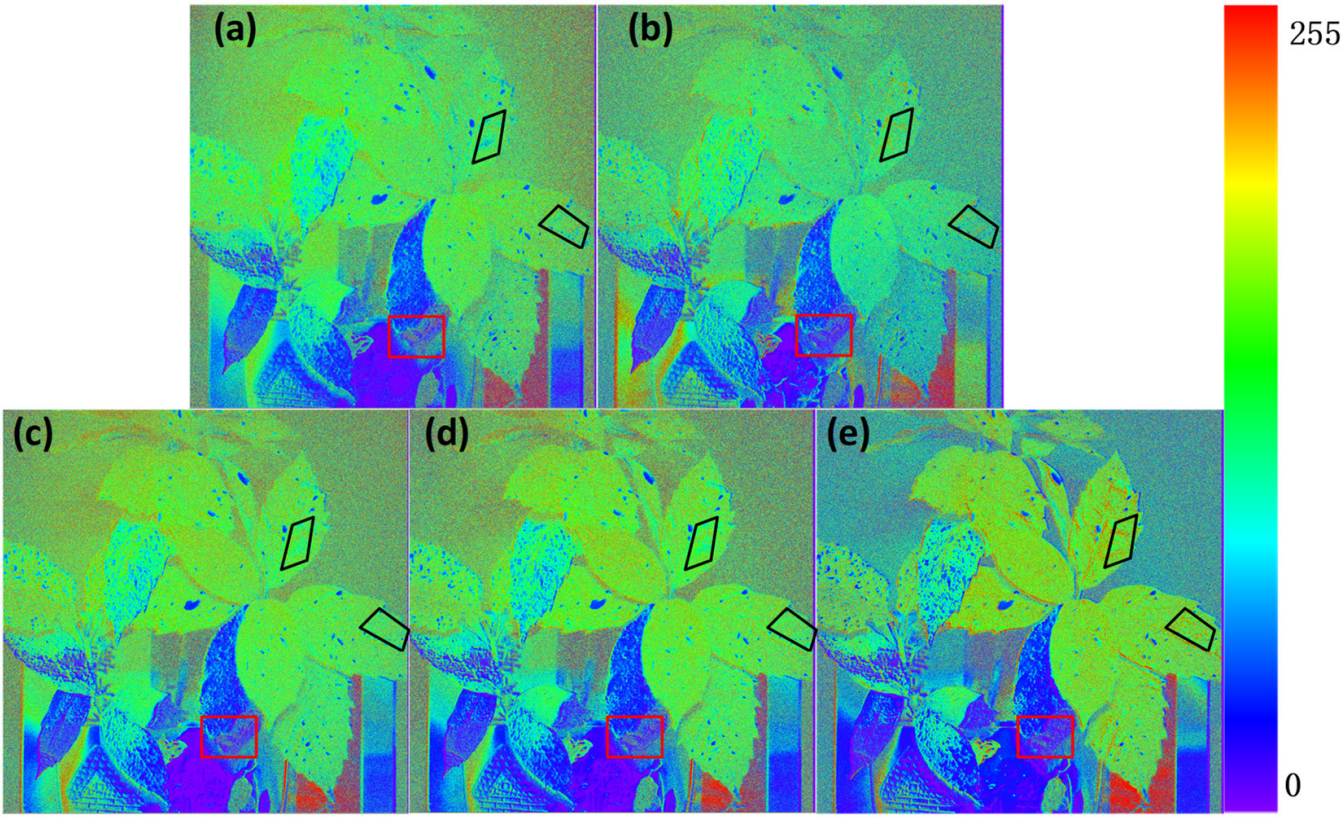

Fig. 20. NSRVI images of different illuminances: (a) NSRVI pseudo-color image of 0.27 lx; (b) NSRVI pseudo-color image of 1.19 lx; (c) NSRVI pseudo-color image of 5.13 lx; (d) NSRVI pseudo-color image of 10.29 lx; and (e) NSRVI pseudo-color image of 102.1 lx.

5.13, 10.29, and 102.1 lx. Fig. 20 shows the NSRVI images under different illumination, and the illumination corresponds to Fig. 20(a): 0.27 lx, Fig. 20(b): 1.19 lx, Fig. 20(c): 5.13 lx, Fig. 20(d): 10.29 lx, and Fig. 20(e): 102.1 lx. In Fig. 20, the specular reflection in the black box has been eliminated, and the value of the withered leaf in the red box is also smaller than that of the stressed grade-3 leaf.

Fig. 21 shows a 2-D scatter diagram of NSRVI image, where x-axis represents the number of groups and y-axis represents the NSRVI value. The illumination corresponds to Fig. 21(a): 0.27 lx, Fig. 21(b): 1.19 lx, Fig. 21(c): 5.13 lx, Fig. 21(d): 10.29 lx, and Fig. 21(e): 102.1 lx. The classification lines are drawn at the mean of the health condition grades of plants. As can be seen from Fig. 21, the two classification lines of healthy leaf and specular reflection leaf under 102.1 lx are almost equal, but the difference between the two classification lines of healthy leaf and specular reflection leaf under 0.27 illuminance is the largest, indicating the best classification results under 102.1 lx and the poorest classification results under 0.27 lx.

The linear correlation between NSRVI and SPAD was analyzed. As shown in Fig. 22, the correlation coefficients between NSRVI and SPAD are 0.27 lx ($R^2 = 0.8$), 1.19 lx ($R^2 = 0.827$), 5.13 lx ($R^2 = 0.861$), 10.29 lx ($R^2 = 0.855$), and 102.1 lx ($R^2 = 0.899$), respectively. With the decrease of illumination, the inversion accuracy of chlorophyll content decreases because the decrease of illumination leads to imaging noise. In addition, our system can still work in a low-light environment, providing a solution for remote sensing monitoring of vegetation health in such an environment. The correlation coefficient (R^2), RMSE, Bias, and P values are shown in Table III.

D. Multiangle Experimental Check

Experiments on NSRVI under two angles are carried out to verify the performance of NSRVI for different angles. As shown in Fig. 23, we chose 30° as the incident zenith angle. Measurements were taken first in the nadir direction and then at forward 30°.

As shown in Fig. 24, the data image obtained from the nadir direction; Fig. 24(a) shows the NDVI image, Fig. 24(b) shows the NDVI pseudo-color image, Fig. 24(c) shows the NSRVI image, and Fig. 24(d) shows the NSRVI pseudo-color image. As shown in Fig. 25, it is the data image obtained in the forward 30° direction; Fig. 25(a) shows the NDVI image, Fig. 25(b) shows the NDVI pseudo-color image, Fig. 25(c) shows the NSRVI image, and Fig. 25(d) shows the NSRVI pseudo-color image. The black box is the selected leaf of interest (healthy leaf). It can be seen that the NDVI value at the position where specular reflection occurs in the black box in Figs. 24(b) and 25(b) is low. The specular reflection interference in Figs. 24(d) and 25(d) has been eliminated.

Three-hundred samples were obtained from the healthy area and the specular area, and then, the two sets of data were averaged and divided, respectively. As shown in Fig. 26, the closer the ratio is to 1, the better the effect of eliminating

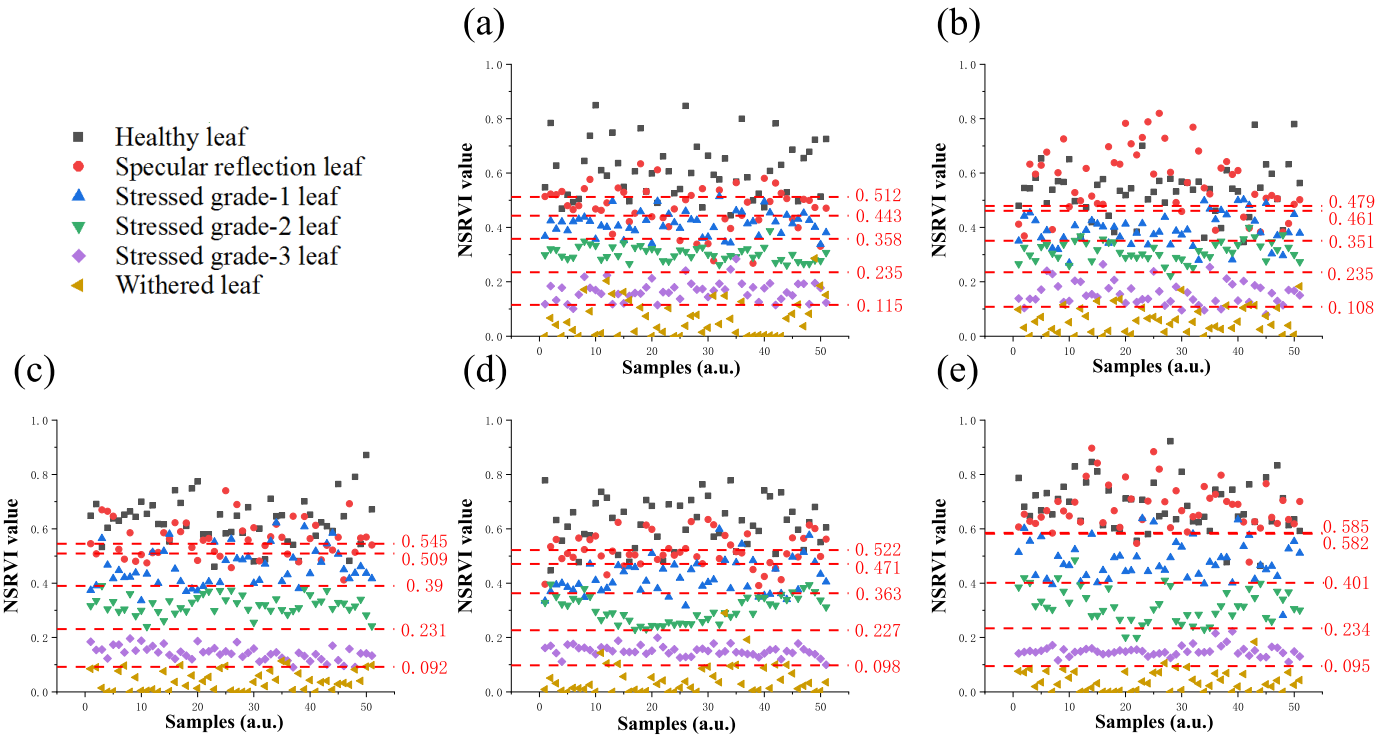

Fig. 21. NSRVI scatterplot: (a) 0.27 lx; (b) 1.19 lx; (c) 5.13 lx; (d) 10.29 lx; and (e) 102.1 lx.

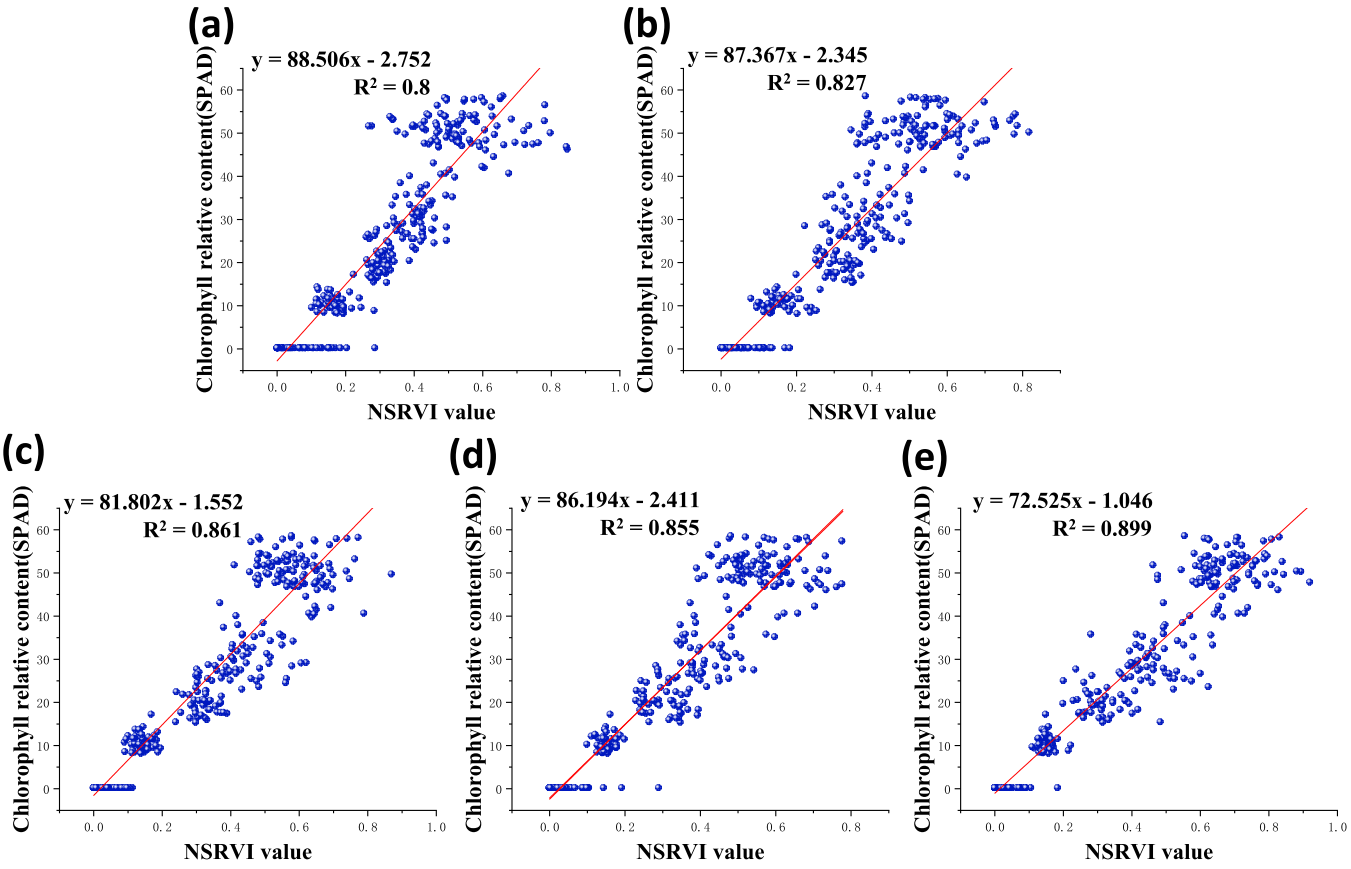

Fig. 22. Correlation of SPAD with NSRVI: (a) 0.27 lx; (b) 1.19 lx; (c) 5.13 lx; (d) 10.29 lx; and (e) 102.1 lx.

specular reflection. It can be seen that the specular reflection cancellation effect of the NSRVI in the nadir direction and forward 30° is very good.

IV. Discussion

Specular reflection is an important source of error for remote tracing of chlorophyll content. An NSRVI was introduced to

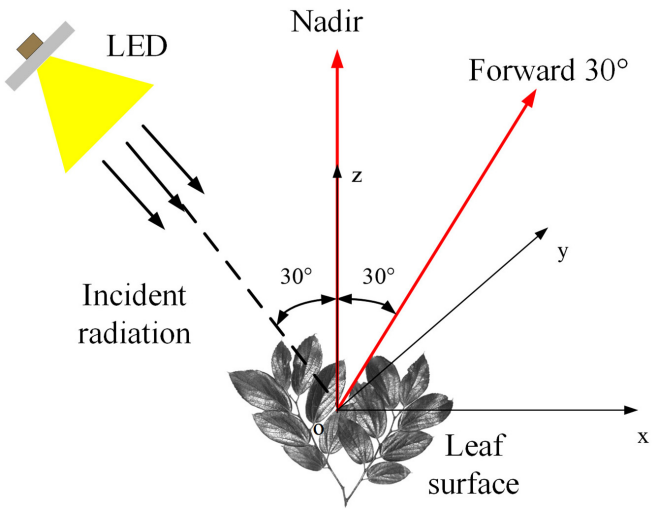

Fig. 23. Schematic of the measurement. The *xoy* plane is the horizontal plane to which the leaf is fixed. The first observation is nadir direction, and the second observation is 30° forward.

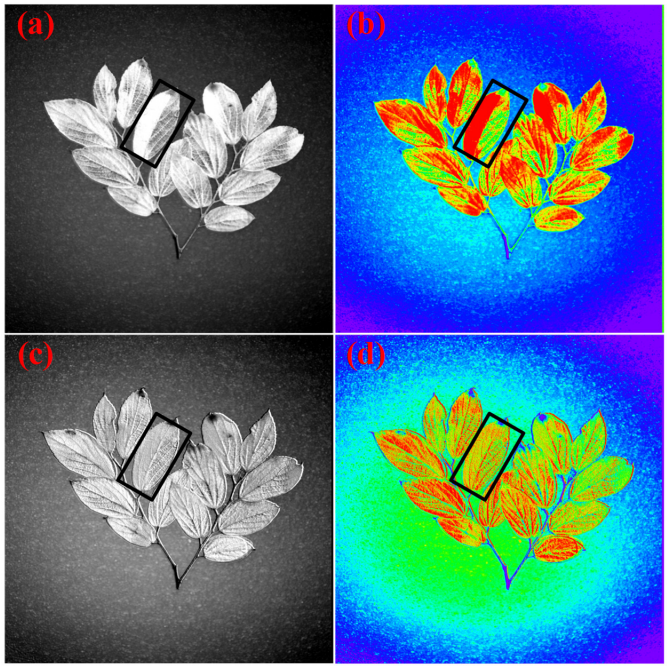

Fig. 24. Nadir direction data image: (a) NDVI image; (b) NDVI pseudo-color image; (c) NSRVI image; and (d) NSRVI pseudo-color image.

eliminate the effect of leaf specular reflection on plant health detection, and a PMSIS was developed to detect the vegetation health condition and evaluate the effect of removing specular reflection from leaves.

A. Interference Mechanism of Leaf Specular Reflection on the Inversion of Vegetation Index Chlorophyll Content

As shown in Fig. 7, the SPAD values of specular and healthy leaf are above 40.59. The specular reflection area is located in the healthy leaf area, which also means that the more specular (visually smoother) the leaf surface, the stronger is the specular reflection. The surface smoothness of leaves is related to their

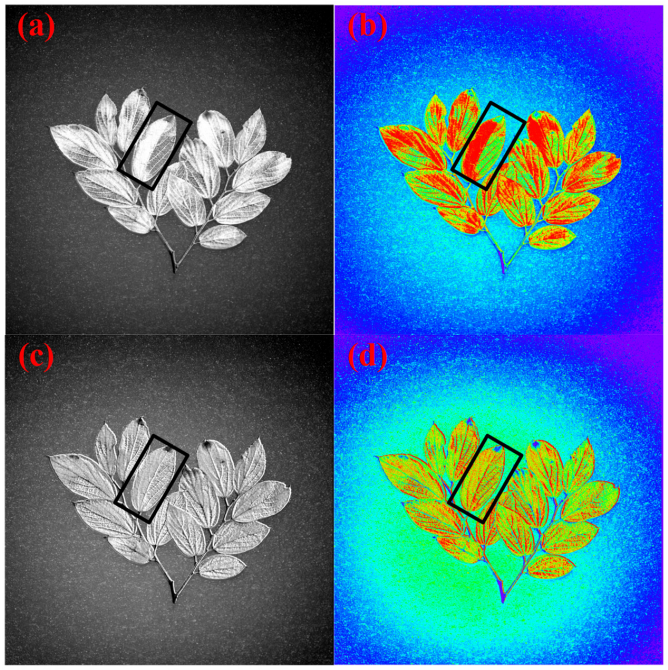

Fig. 25. Forward 30° data image: (a) NDVI image; (b) NDVI pseudo-color image; (c) NSRVI image; and (d) NSRVI pseudo-color image.

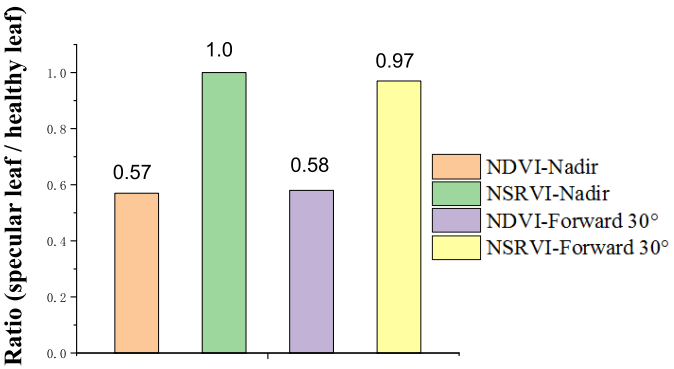

Fig. 26. Histogram of the ratio of specular to healthy leaf for NDVI and NSRVI in the nadir and forward 30° direction.

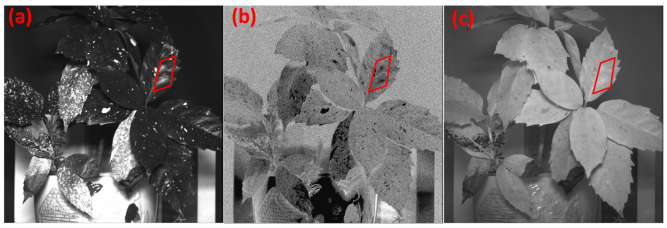

Fig. 27. Images recorded from spotted laurel: (a) 680-nm image; (b) DoLP image; and (c) 760-nm image.

health status, that is, the healthier the leaf, the smoother is the surface. It can be seen from the red boxes in Fig. 27(a) and (c) that the specular reflection of leaf was found in the 680-nm spectral measurement, and such brightness overwhelms their natural color. The reflectance image at 760 nm is not sensitive to the specular reflection. This is why the values of the specular reflection area are very low in SR images and NDVI images.

However, the value of the specular reflection area in the red box in Fig. 27(b) is very low, which indicates that DoLP and $R_{680\ \mathrm{nm}}$ change in a trend opposite to each other, which is also consistent with previous studies [56], [57].

In remote sensing monitoring, the reflectance of leaves is composed of two parts: specular reflectance and diffuse reflectance [58]. Specular reflection originates from direct reflection from the leaves surface, and incident light does not penetrate the interior of the leaves to interact with pigments and mesophyll structures within the leaves [37]. Therefore, the specular component does not carry leaf biochemical information [59]. Diffuse reflection comes from the interior of leaf, and the spectral variation of diffuse reflection depends on the biochemical composition. Therefore, the existence of leaf specular reflection may lead to interference in the remote detection of chlorophyll content. The black frame area in Fig. 8 shows the interference caused by the specular reflection, which makes the healthy leaf mistaken for the stressed leaf [Fig. 9(a) and (b)]. In addition, the specular reflection interference of leaf greatly reduced the chlorophyll inversion accuracy, and the correlation between SPAD and SR was only 0.456, and that between SPAD and NDVI was 0.625. This detrimental effect can also be seen in Table II, with a sensitivity of 0% and a specificity of 0% for the classification of specular reflection leaf from stressed grade-1 leaf.

B. Differences in Sensitivity to Specular Reflections Between Vegetation Indices

Due to the sensitivity of SR and NDVI to specular reflections, Sims and Gamon [40] introduced mSR and mNDVI to mitigate the effects of specular reflections [see (7) and (8)]. This study also confirmed that mSR and mNDVI indices had a better performance than SR and NDVI indices, and Fig. 13 illustrates the effectiveness of this strategy. However, since $R_{445\ \mathrm{nm}}$ contains both diffuse and specular reflections, the value of $R_{445\ \mathrm{nm}}$ is higher than the specular reflectance. In mSR and mNDVI, the $R_{445\ \mathrm{nm}}$ reflectance is taken as a measure of the specular reflection of leaf and is subtracted to remove specular reflection interference. Therefore, the values of the specular reflections of mSR and mNDVI are larger than those of healthy leaf (the black-frame area in Fig. 11). In addition, this method makes the value of the withered leaf higher than the stressed grade-3 leaf (the red-frame area in Fig. 11), which leads to a decrease in the chlorophyll retrieval accuracy. Therefore, mSR and mNDVI are not particularly ideal in eliminating specular reflection effects.

Studies have shown that the main source of the polarized reflectivity of leaves is the specular reflectance of leaves [60]. Therefore, Li et al. [45] simply obtains the specular component of the leaves by multiplying the polarized reflectance (R_p) by the constant c, which is a simplification of the actual situation, without considering the influence of leaves' roughness, such as shadows [61]. However, this method does not completely eliminate the specular reflection when the light from the specular reflection of the leaf overwhelms their natural color (see the black-frame area in Fig. 14).

However, we developed an NSRVI [see (14)] that almost completely eliminates the specular reflection of leaf

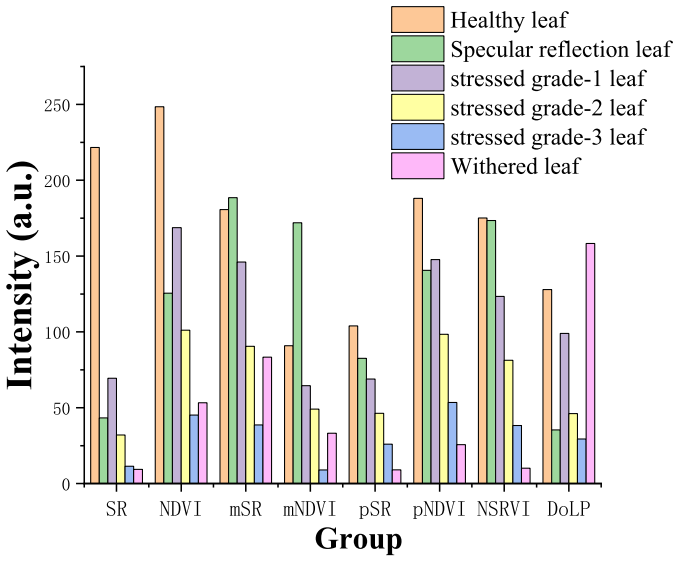

Fig. 28. Histograms of different health conditions for SR, NDVI, mSR, mNDVI, pSR, pNDVI, NSRVI, and DoLP.

(the black-frame area in Fig. 17). It can be seen from Fig. 18 that the specular reflection area is located in the healthy leaf area, and the various health grades of the vegetation are well-classified. The correlation coefficient between SPAD and NSRVI is 0.899, indicating the effectiveness of our method in eliminating specular reflection of leaf. The NSRVI data were used to draw a scatterplot (Fig. 18) to classify different grades of vegetation health condition. The accuracy of classification is shown in Table II, from which we can see that the sensitivity and specificity of NSRVI for the classification of vegetation with different conditions are generally higher than those of mSR, mNDVI, pSR, and pNDVI. Furthermore, in applying NSRVI in distinguishing specular reflection leaf from the stressed grade-1 leaf, the sensitivity was 92% and the specificity was 96%, which is significant as they demonstrate the potential of NSRVI in removing specular reflections from leaves. It can be seen from Table III that when the illuminance is 102.1 lx, the RMSE and Bias of NSRVI are the smallest, 6.1603 and 0.0011, respectively. This also indicates that the use of NSRVI for plant health monitoring has the smallest error and the highest accuracy.

C. Interference of Withered Leaf on Vegetation Health Monitoring

The portable chlorophyll detector penetrates the leaves through two kinds of light, and finally calculates the SPAD value and indicates it on the display screen. Because the light transmittance of withered leaf is almost 0, the portable chlorophyll detector cannot detect their SPAD. In addition, the withered leaf in this article is completely withered leaf, so we set their SPAD value to 0.

As shown in Fig. 28, withered leaf and stressed grade-3 leaf in SR and NDVI were confused with each other, which can also be seen in the SR and NDVI scatterplots (Fig. 9). This is because withered leaf has no biochemical characteristics, so SR and NDVI cannot detect withered leaf. However, the

values of withered leaf in mSR and mNDVI were larger than those of stressed grade-3 leaf (the red-frame area in Fig. 11; Fig. 12), which was abnormal. Because withered leaf no longer has biochemical characteristics, their values are the same as the background values in all bands. Under stress, the reduction of mSR and mNDVI values was related to the reduction of SPAD content, and the optical properties of leaves can help decipher this proportional relationship. Compared with healthy ones, leaves of stressed plants had lower SPAD content [62], and decreased chlorophyll content resulted in decreased chlorophyll absorption at $R_{680\ \mathrm{nm}}$ and $R_{445\ \mathrm{nm}}$ ($R_{680\ \mathrm{nm}}$ decreased more than $R_{445\ \mathrm{nm}}$), enhanced reflectance, and decreased reflectance at $R_{760\ \mathrm{nm}}$. According to (7) and (8), it can be known that the value of stressed grade-3 leaf must be lower than the background value. Therefore, the values of withered leaf in mSR and mNDVI were greater than those of stressed grade-3 leaf.

As shown in Figs. 14, 17, and 28, the values of withered leaf in pSR, pNDVI, and NSRVI are lower than those of stressed grade-3 leaf, which is correct. The higher DoLP value of the withered leaf is because their surface roughness has lower reflectance, and their DOLP is higher because of the inverse proportional relationship between the DoLP of the target and the surface reflectance [63]. Therefore, DoLP facilitates the detection of withered leaf. It can be seen from (12)–(14) that after adding DoLP to the formula, the values of withered leaf calculated by pSR, pNDVI, and NSRVI are lower than those of stressed grade-3 leaf, so that withered leaf and stressed grade-3 leaf are correctly distinguished.

D. Influence of Illumination on NSRVI

Li et al. [49] came up with the night plant status detection index (NPSDI), a new index for characterizing the status of plants at night, to detect the physiological condition of vegetation at night. At present, most of the remote sensing research is carried out in the light environment, and there are few related researches on the monitoring of vegetation health status at night. Therefore, based on the previous research results, we conducted experiments on NSRVI under different illumination to verify that NSRVI can be used in different illumination environments. It can be clearly seen in Fig. 22 that with the increase of illuminance, the correlation R^2 between SPAD and NSRVI gradually increases (Table III). In a low-light-level environment, the system imaging generates noise under the impact of illumination, so the chlorophyll inversion accuracy is reduced. However, even if the environmental illuminance is 0.27 lx, the chlorophyll inversion accuracy was still high ($R^2 = 0.8$ and RMSE $= 8.678$), showing the potential of applying the NSRVI determined by PMSIS imaging to understand the condition of vegetation at night from a proximal sensing platform.

E. Potential Applications of Our Method to Canopy Chlorophyll Inversion

At present, the system can only monitor the vegetation health condition statically because we choose to rotate the polarization measurement manually. Of course, this also increases the error of polarization measurement. The PMSIS imaging is a passive technique, so it does not require a laser to excite fluorescence like fluorescence lidar. In addition, only a compact instrument is required, which is less expensive. In the future, we will develop devices for dynamic measurement that can be deployed on platforms (such as cars, unmanned aerial vehicle (UAV), and satellites) to eliminate specular reflections while sensing the effects of various types of biological and abiotic pressures on farmland and forests from a distance. When measuring in the field, the specular reflection interference may be more serious, which is also an area our efforts will be put in in the future.

V. Conclusion

In this article, a polarization-based system of PMSIS is developed and a NSRVI is proposed to eliminate the specular reflection interference of vegetation and improve the accuracy in detecting plant health condition. To check the ability to eliminate specular reflection interference and monitor plant health condition via NSRVI, the spotted laurel leaves in different conditions were measured and analyzed. The changes of SPAD, SR, NDVI, mSR, mNDVI, pSR, pNDVI, and NSRVI at different grades of plant health condition were measured, and spotted laurel leaves were also classified based on their health condition. The NSRVI value decreases as the plant health status declines, and it is positively correlated with the SPAD of spotted laurel. The correlation coefficient between NSRVI and SPAD is 0.889. A preliminary study on the classification of different grades of vegetation condition by using the scatterplot of NSRVI shows that the sensitivity and specificity of the classification of specular reflection leaf from stressed grade-1 leaf are 92% and 96%, respectively, indicating that this method is very effective in eliminating the interference of specular reflection of plants.

The results show the following.

1) SR and NDVI monitoring of plant health condition are most disturbed by the specular reflection of leaf.
2) The improved mSR and mNDVI can eliminate part of the specular reflection interference, but the interference by withered leaf tends to be larger than that by the stressed grade-3 leaf, resulting in errors.
3) pSR and pNDVI can eliminate some specular reflection interference and correct the error between withered leaf and stressed grade-3 leaf.
4) NSRVI has the best performance in eliminating specular reflection interference, and the correlation coefficient between NPSDI and SPAD is 0.889. NSRVI can almost completely eliminate specular reflection interference and correct the error between withered leaf and stressed grade-3 leaf.
5) Different illumination experiments of NSRVI show that with the decrease of illumination, the inversion accuracy of chlorophyll content decreases, and the reason lies in that the decrease of illumination leads to the generation of imaging noise. Even if the environment illuminance is 0.27 lx, the chlorophyll inversion accuracy is still high ($R^2 = 0.8$), showing the potential to apply the

NSRVI determined by PMSIS imaging in detecting the pant health condition amid a low-light-level environment from a near-end sensing platform.

In summary, the NSRVI proposed in this article can effectively eliminate the specular reflection interference and improve the accuracy in monitoring vegetation health condition. The method is reliable even under adversely low-light-level conditions. It provides a good idea for biochemical retrieval at the canopy scale and deserves further study.

ACKNOWLEDGMENT

Thanks to the colleagues and students who participated in the outdoor data collection. The authors would also like to thank the anonymous reviewers for their detailed and constructive comments on this article.

REFERENCES

[1] D. Haboudane, J. R. Miller, E. Pattey, P. J. Zarco-Tejada, and I. B. Strachan, "Hyperspectral vegetation indices and novel algorithms for predicting green LAI of crop canopies: Modeling and validation in the context of precision agriculture," *Remote Sens. Environ.*, vol. 90, no. 3, pp. 337–352, 2004.

[2] S. W. Running and S. T. Gower, "FOREST-BGC, a general model of forest ecosystem processes for regional applications. II. Dynamic carbon allocation and nitrogen budgets," *Tree Physiol.*, vol. 9, nos. 1–2, pp. 147–160, Jul. 1991.

[3] H. Croft et al., "The global distribution of leaf chlorophyll content," *Remote Sens. Environ.*, vol. 236, Jan. 2020, Art. no. 111479.

[4] S. L. Ustin et al., "Retrieval of foliar information about plant pigment systems from high resolution spectroscopy," *Remote Sens. Environ.*, vol. 113, pp. S67–S77, Sep. 2009.

[5] B. Yang, L. Qin, J. Liu, and X. Liu, "UTRNet: An unsupervised time-distance-guided convolutional recurrent network for change detection in irregularly collected images," *IEEE Trans. Geosci. Remote Sens.*, vol. 60, pp. 1–16, 2022.

[6] C. Wu, Z. Niu, Q. Tang, and W. Huang, "Estimating chlorophyll content from hyperspectral vegetation indices: Modeling and validation," *Agricult. Forest Meteorol.*, vol. 148, pp. 1230–1241, Jul. 2008.

[7] J. P. Palta, "Leaf chlorophyll content," *Remote Sens. Rev.*, vol. 5, no. 1, pp. 207–213, Jan. 1990.

[8] P. J. Zarco-Tejada, A. Hornero, P. S. A. Beck, T. Kattenborn, P. Kempeneers, and R. Hernández-Clemente, "Chlorophyll content estimation in an open-canopy conifer forest with Sentinel-2A and hyperspectral imagery in the context of forest decline," *Remote Sens. Environ.*, vol. 223, pp. 320–335, Mar. 2019.

[9] S. C. Thomas, "Increased leaf reflectance in tropical trees under elevated CO_2," *Global Change Biol.*, vol. 11, no. 2, pp. 197–202, Feb. 2005.

[10] S. R. Sandmeier, "Acquisition of bidirectional reflectance factor data with field goniometers," *Remote Sens. Environ.*, vol. 73, no. 3, pp. 257–269, Sep. 2000.

[11] R. C. Sharma, K. Kajiwara, and Y. Honda, "Estimation of forest canopy structural parameters using kernel-driven bi-directional reflectance model based multi-angular vegetation indices," *ISPRS J. Photogramm. Remote Sens.*, vol. 78, pp. 50–57, Apr. 2013.

[12] J. Yue, G. Yang, Q. Tian, H. Feng, K. Xu, and C. Zhou, "Estimate of winter-wheat above-ground biomass based on UAV ultrahigh-ground-resolution image textures and vegetation indices," *ISPRS J. Photogramm. Remote Sens.*, vol. 150, pp. 226–244, Apr. 2019.

[13] L. Gao et al., "Remote sensing algorithms for estimation of fractional vegetation cover using pure vegetation index values: A review," *ISPRS J. Photogramm. Remote Sens.*, vol. 159, pp. 364–377, Jan. 2020.

[14] H. K. Lichtenthaler and A. R. Wellburn, "Determinations of total carotenoids and chlorophylls A and B of leaf extracts in different solvents," *Biochem. Soc. Trans.*, vol. 11, pp. 591–592, May 1983.

[15] A. C. Madeira, A. Mentions, M. E. Ferreira, and M. D. L. Taborda, "Relationship between spectroradiometric and chlorophyll measurements in green beans," *Commun. Soil Sci. Plant Anal.*, vol. 31, nos. 5–6, pp. 631–643, Mar. 2000.

[16] A. A. Gitelson, Y. Gritz, and M. N. Merzlyak, "Relationships between leaf chlorophyll content and spectral reflectance and algorithms for non-destructive chlorophyll assessment in higher plant leaves," *J. Plant Physiol.*, vol. 160, no. 3, pp. 271–282, 2003.

[17] Y. Zhang, J. M. Chen, J. R. Miller, and T. L. Noland, "Leaf chlorophyll content retrieval from airborne hyperspectral remote sensing imagery," *Remote Sens. Environ.*, vol. 112, no. 7, pp. 3234–3247, Jul. 2008.

[18] J. M. Bioucas-Dias, A. Plaza, G. Camps-Valls, P. Scheunders, N. M. Nasrabadi, and J. Chanussot, "Hyperspectral remote sensing data analysis and future challenges," *IEEE Geosci. Remote Sens. Mag.*, vol. 1, no. 2, pp. 6–36, Jun. 2013.

[19] G. V. G. Baranoski and J. G. Rokne, "A practical approach for estimating the red edge position of plant leaf reflectance," *Int. J. Remote Sens.*, vol. 26, no. 3, pp. 503–521, Feb. 2005.

[20] C. F. Jordan, "Derivation of leaf-area index from quality of light on the forest floor," *Ecology*, vol. 50, no. 4, pp. 663–666, 1969.

[21] J. W. Rouse, R. H. Hass, J. A. Schell, and D. W. Deering, "Monitoring vegetation systems in the great plains with ERTS," in *Proc. 3rd ERTS Symp.*, vol. 1, 1973, pp. 309–317.

[22] A. D. Richardson, S. P. Duigan, and G. P. Berlyn, "An evaluation of noninvasive methods to estimate foliar chlorophyll content," *New Phytologist*, vol. 153, no. 1, pp. 185–194, Jan. 2002.

[23] C. Wang et al., "A snow-free vegetation index for improved monitoring of vegetation spring green-up date in deciduous ecosystems," *Remote Sens. Environ.*, vol. 196, pp. 1–12, Jul. 2017.

[24] P. Yang, C. van der Tol, P. K. E. Campbell, and E. M. Middleton, "Fluorescence correction vegetation index (FCVI): A physically based reflectance index to separate physiological and non-physiological information in far-red sun-induced chlorophyll fluorescence," *Remote Sens. Environ.*, vol. 240, Apr. 2020, Art. no. 111676.

[25] W. Wei et al., "Temperature vegetation precipitation dryness index (TVPDI)-based dryness-wetness monitoring in China," *Remote Sens. Environ.*, vol. 248, Oct. 2020, Art. no. 111957.

[26] L. N. Huo, H. J. Persson, and E. Lindberg, "Early detection of forest stress from European spruce bark beetle attack, and a new vegetation index: Normalized distance red & SWIR (NDRS)," *Remote Sens. Environ.*, vol. 255, Mar. 2021, Art. no. 112240.

[27] A. A. Gitelson and M. N. Merzlyak, "Signature analysis of leaf reflectance spectra: Algorithm development for remote sensing of chlorophyll," *J. Plant Physiol.*, vol. 148, nos. 3–4, pp. 494–500, 1996.

[28] A. A. Gitelson, M. N. Merzlyak, and H. K. Lichtenthaler, "Detection of red edge position and chlorophyll content by reflectance measurements near 700 nm," *J. Plant Physiol.*, vol. 148, nos. 3–4, pp. 501–508, Jan. 1996.

[29] A. A. Gitelson, Y. J. Kaufman, and M. N. Merzlyak, "Use of a green channel in remote sensing of global vegetation from EOS-MODIS," *Remote Sens. Environ.*, vol. 58, no. 3, pp. 289–298, 1996.

[30] B. J. Yoder and R. H. Waring, "The normalized difference vegetation index of small douglas-fir canopies with varying chlorophyll concentrations," *Remote Sens. Environ.*, vol. 49, no. 1, pp. 81–91, Jul. 1994.

[31] C. Buschmann and E. Nagel, "*In vivo* spectroscopy and internal optics of leaves as basis for remote sensing of vegetation," *Int. J. Remote Sens.*, vol. 14, no. 4, pp. 711–722, Mar. 1993.

[32] H. K. Lichtenthaler, A. Gitelson, and M. Lang, "Non-destructive determination of chlorophyll content of leaves of a green and an aurea mutant of tobacco by reflectance measurements," *J. Plant Physiol.*, vol. 148, nos. 3–4, pp. 483–493, Jan. 1996.

[33] A. Yagci, L. Di, and M. Deng, "The effect of corn–soybean rotation on the NDVI-based drought indicators: A case study in Iowa, USA, using vegetation condition index," *GISci. Remote Sens.*, vol. 52, no. 3, pp. 290–314, 2015.

[34] Y. Liu et al., "Evaluation of consistency among three NDVI products applied to high mountain Asia in 2000–2015," *Remote Sens. Environ.*, vol. 269, Feb. 2022, Art. no. 112821.

[35] B. Datt, "A new reflectance index for remote sensing of chlorophyll content in higher plants: Tests using eucalyptus leaves," *J. Plant Physiol.*, vol. 154, no. 1, pp. 30–36, Jan. 1999.

[36] M. Prabhakar et al., "Hyperspectral indices for assessing damage by the solenopsis mealybug (hemiptera: Pseudococcidae) in cotton," *Comput. Electron. Agricult.*, vol. 97, pp. 61–70, Sep. 2013.

[37] L. Grant, "Diffuse and specular characteristics of leaf reflectance," *Remote Sens. Environ.*, vol. 22, no. 2, pp. 309–322, Jul. 1987.

[38] V. C. Vanderbilt, L. Grant, L. L. Biehl, and B. F. Robinson, "Specular, diffuse, and polarized light scattered by two wheat canopies," *Appl. Opt.*, vol. 24, no. 15, pp. 2408–2418, Aug. 1985.

[39] L. Bousquet, S. Lachérade, S. Jacquemoud, and I. Moya, "Leaf BRDF measurements and model for specular and diffuse components differentiation," *Remote Sens. Environ.*, vol. 98, nos. 2–3, pp. 201–211, Oct. 2005.
[40] D. A. Sims and J. A. Gamon, "Relationships between leaf pigment content and spectral reflectance across a wide range of species, leaf structures and developmental stages," *Remote Sens. Environ.*, vol. 81, nos. 2–3, pp. 337–354, Aug. 2002.
[41] J.-B. Féret, A. A. Gitelson, S. D. Noble, and S. Jacquemoud, "PROSPECT-D: Towards modeling leaf optical properties through a complete lifecycle," *Remote Sens. Environ.*, vol. 193, pp. 204–215, May 2017.
[42] K. M. Barry and G. J. Newnham, "Quantification of chlorophyll and carotenoid pigments in eucalyptus foliage with the radiative transfer model PROSPECT 5 is affected by anthocyanin and epicuticular waxes," GSR_2 Geospatial Sci. Res._2, Melbourne, VIC, Australia, Dec. 2012, pp. 1–7. [Online]. Available: http://ecite.utas.edu.au/78991
[43] D. Xie, P. Wang, W. Qin, Q. Zhu, and J. Wang, "A Study on the radiance distribution in the canopy affected by non-Lambert characteristics of leaf based on RGM," *J. Remote Sens.*, vol. 11, pp. 868–874, Nov. 2007.
[44] S. Jacquemoud et al., "PROSPECT + SAIL models: A review of use for vegetation characterization," *Remote Sens. Environ.*, vol. 113, pp. S56–S66, Sep. 2009.
[45] Y. Li, Y. Chen, and J. Huang, "An approach to improve leaf pigment content retrieval by removing specular reflectance through polarization measurements," *IEEE Trans. Geosci. Remote Sens.*, vol. 57, no. 4, pp. 2173–2186, Apr. 2019.
[46] S. Wang, C. Yu, Y. Sun, F. Gao, and J. Dong, "Specular reflection removal of ocean surface remote sensing images from UAVs," *Multimedia Tools Appl.*, vol. 77, no. 9, pp. 11363–11379, 2018.
[47] Y. Li and J. Huang, "Remote sensing of pigment content at a leaf scale: Comparison among some specular removal and specular resistance methods," *Remote Sens.*, vol. 11, no. 8, p. 983, Apr. 2019.
[48] D. Li et al., "PROCWT: Coupling PROSPECT with continuous wavelet transform to improve the retrieval of foliar chemistry from leaf bidirectional reflectance spectra," *Remote Sens. Environ.*, vol. 206, pp. 1–14, Mar. 2018.
[49] S. Li, J. Jiao, and C. Wang, "Research on polarized multi-spectral system and fusion algorithm for remote sensing of vegetation status at night," *Remote Sens.*, vol. 13, no. 17, p. 3510, Sep. 2021.
[50] L. Zhang, X. Sun, T. Wu, and H. Zhang, "An analysis of shadow effects on spectral vegetation indexes using a ground-based imaging spectrometer," *IEEE Geosci. Remote Sens. Lett.*, vol. 12, no. 11, pp. 2188–2192, Nov. 2015.
[51] B. Yang, H. Zhao, and W. Chen, "Semi-empirical models for polarized reflectance of land surfaces: Intercomparison using space-borne POLDER measurements," *J. Quant. Spectrosc. Radiat. Transf.*, vol. 202, pp. 13–20, Nov. 2017.
[52] B. Yang, L. Yan, and S. Liu, "Polarization of light reflected by grass: Modeling using visible-sunlit areas," *Photogramm. Eng. Remote Sens.*, vol. 86, no. 12, pp. 745–752, Dec. 2020.
[53] J. R. Schott, *Fundamentals of Polarimetric Remote Sensing*, vol. 81. Bellingham, WA, USA: SPIE, 2009.
[54] D. Lavigne, M. Breton, G. Fournier, M. Pichette, and V. Rivet, "Development of performance metrics to characterize the degree of polarization of man-made objects using passive polarimetric images," *Proc. SPIE*, vol. 7336, May 2009, Art. no. 73361A.
[55] S. Liu, L. Yan, and B. Yang, "Degree of linear polarization of land surfaces: Analyses using POLDER/PARASOL measurements," *IEEE Access*, vol. 8, pp. 200561–200572, 2020.
[56] L. Grant, C. S. T. Daughtry, and V. C. Vanderbilt, "Polarized and non-polarized leaf reflectances of coleus blumei," *Environ. Exp. Botany*, vol. 27, no. 2, pp. 139–145, Apr. 1987.
[57] L. Grant, C. S. T. Daughtry, and V. C. Vanderbilt, "Polarized and specular reflectance variation with leaf surface features," *Physiol. Plant*, vol. 88, no. 1, pp. 1–9, 1993.
[58] J. T. Woolley, "Reflectance and transmittance of light by leaves," *Plant Physiol.*, vol. 47, no. 5, pp. 656–662, 1971.
[59] G. Rondeaux and V. C. Vanderbilt, "Specularly modified vegetation indices to estimate photosynthetic activity," *Int. J. Remote Sens.*, vol. 14, no. 9, pp. 1815–1823, 1993.
[60] C. C. Bell and P. J. Curran, "The effect of specular reflectance on the relationship between reflectance and vegetation amount," *Int. J. Remote Sens.*, vol. 13, no. 14, pp. 2751–2757, 1992.
[61] K. E. Torrance and E. M. Sparrow, "Theory for off-specular reflection from roughened surfaces," *J. Opt. Soc. Amer.*, vol. 57, no. 9, pp. 1105–1114, 1967.
[62] S. N. Raji et al., "Detection of mosaic virus disease in cassava plants by sunlight-induced fluorescence imaging: A pilot study for proximal sensing," *Int. J. Remote Sens.*, vol. 36, no. 11, pp. 2880–2897, Jun. 2015.
[63] D. H. Goldstein, "Polarimetric characterization of federal standard paints," *Proc. SPIE*, vol. 4133, pp. 112–123, 2000.

Siyuan Li received the B.S. degree from the Henan University of Technology, Zhengzhou, China, in 2018. He is currently pursuing the Ph.D. degree with Shanghai University, Shanghai, China.

His research interests include remote sensing of plant biochemistry.

Jiannan Jiao received the B.S. degree from Jilin University, Changchun, China, in 2013, the M.S. degree from Peking University, Beijing, China, in 2016, and the Ph.D. degree from Nanyang Technological University, Singapore, in 2020.

His research interests focus on optical sensing and instrumentation.

Jinbo Chen received the Ph.D. degree from Shanghai University, Shanghai, China, in 2014.

He is currently working as a Lecturer with the School of Mechatronic Engineering and Automation, Shanghai University. His research interests include computer vision and remote sensing.

Chi Wang received the Ph.D. degree from Tianjin University, Tianjin, China, in 2009.

He is currently a Professor with Shanghai University, Shanghai, China. His main research interests include optical fiber sensing and precision measurement technology.